Molecular Therapy
Original Article

Short-Term Local Expression of a PD-L1 Blocking Antibody from a Self-Replicating RNA Vector Induces Potent Antitumor Responses

Maria Cristina Ballesteros-Briones,[1] Eva Martisova,[1] Erkuden Casales,[1] Noelia Silva-Pilipich,[1] Maria Buñuales,[1] Javier Galindo,[1] Uxua Mancheño,[2] Marta Gorraiz,[2] Juan J. Lasarte,[2] Grazyna Kochan,[3] David Escors,[3] Alfonso R. Sanchez-Paulete,[2] Ignacio Melero,[2,4,5] Jesus Prieto,[1] Ruben Hernandez-Alcoceba,[1] Sandra Hervas-Stubbs,[2] and Cristian Smerdou[1]

[1]Division of Gene Therapy and Regulation of Gene Expression, Cima Universidad de Navarra and Instituto de Investigación Sanitaria de Navarra (IdISNA), 31008 Pamplona, Spain; [2]Division of Immunology and Immunotherapy, Cima Universidad de Navarra and Instituto de Investigación Sanitaria de Navarra (IdISNA), 31008 Pamplona, Spain; [3]Department of Oncology, Navarrabiomed-Biomedical Research Centre, IdiSNA, 31008 Pamplona, Spain; [4]Department of Immunology and Immunotherapy, Clinica Universidad de Navarra, 31008 Pamplona, Spain; [5]Centro de Investigación Biomédica en Red de Cáncer (CIBERONC), 28029 Madrid, Spain

Immune checkpoint blockade has shown anti-cancer efficacy, but requires systemic administration of monoclonal antibodies (mAbs), often leading to adverse effects. To avoid toxicity, mAbs could be expressed locally in tumors. We developed adeno-associated virus (AAV) and Semliki Forest virus (SFV) vectors expressing anti-programmed death ligand 1 (aPDL1) mAb. When injected intratumorally in MC38 tumors, both viral vectors led to similar local mAb expression at 24 h, diminishing quickly in SFV-aPDL1-treated tumors. However, SFV-aPDL1 induced >40% complete regressions and was superior to AAV-aPDL1, as well as to aPDL1 mAb given systemically or locally. SFV-aPDL1 induced abscopal effects and was also efficacious against B16-ovalbumin (OVA). The higher SFV-aPDL1 antitumor activity could be related to local upregulation of interferon-stimulated genes because of SFV RNA replication. This was confirmed by combining local SFV-LacZ administration and systemic aPDL1 mAb, which provided higher antitumor effects than each separated agent. SFV-aPDL1 promoted tumor-specific CD8 T cells infiltration in both tumor models. In MC38, SFV-aPDL1 upregulated co-stimulatory markers (CD137/OX40) in tumor CD8 T cells, and its combination with anti-CD137 mAb showed more pronounced antitumor effects than each single agent. These results indicate that local transient expression of immunomodulatory mAbs using non-propagative RNA vectors inducing type I interferon (IFN-I) responses represents a potent and safe approach for cancer treatment.

INTRODUCTION

Immunotherapy has recently revolutionized the field of cancer therapy, representing one of the most significant breakthroughs in the fight against cancer.[1] Immunotherapies based on the use of monoclonal antibodies (mAbs) able to block immune checkpoints, or genetically engineered T cells able to recognize tumor antigens, are now allowing to treat and cure many tumors previously refractory to conventional therapies.[2]

Among immune checkpoints, the programmed death 1 (PD-1)/programmed death ligand 1 (PD-L1) axis constitutes an important regulator of immune responses.[3,4] PD-1 is usually expressed on activated T cells, whereas its ligand PD-L1 is mainly expressed on the surface of antigen-presenting cells (APCs) and cells in inflamed tissues. The interaction of PD-1 with PD-L1 leads to inhibition of T cells, hampering their effector activity. Importantly, PD-L1 is overexpressed in many cancer cells, allowing tumors to escape immune system recognition.[3,5] Blocking PD-1/PD-L1 interaction with mAbs against either PD-1 or PD-L1 has shown an impressive clinical efficacy against different types of tumors, such as metastatic melanoma, non-small-cell lung cancer, renal cancer, bladder cancer, and Hodgkin's lymphoma.[6] Despite these remarkable therapeutic effects, immunomodulatory mAbs are not effective in all patients and are ineffective in some tumor types, such as pancreatic or microsatellite stable (MSS) colon cancer. In addition, by interfering with natural mechanisms of immune regulation, immunomodulatory mAbs given intravenously frequently cause immune-mediated adverse effects.[7,8]

One possibility to prevent or limit these adverse reactions could be based on administration of mAbs locally in tumors.[9,10] In fact, both preclinical[11] and clinical studies have shown that it is possible to obtain

Received 21 February 2019; accepted 6 September 2019;
https://doi.org/10.1016/j.ymthe.2019.09.016.

Correspondence: Cristian Smerdou, Division of Gene Therapy and Regulation of Gene Expression, Cima Universidad de Navarra and Instituto de Investigación Sanitaria de Navarra (IdISNA), Av. Pio XII 55, 31008 Pamplona, Spain.
E-mail: csmerdou@unav.es
Correspondence: Sandra Hervas-Stubbs, Division of Immunology and Immunotherapy, Cima Universidad de Navarra and Instituto de Investigación Sanitaria de Navarra (IdISNA), Av. Pio XII 55, 31008 Pamplona, Spain.
E-mail: mshervas@unav.es

therapeutic benefit with intratumor injection of mAbs.[12] In these cases, much lower amounts of mAbs would be needed, because their action could be concentrated on the tumor tissue, limiting also in this way their toxicity. This could be particularly interesting when using combinations of different immune checkpoint blockers, like those against PD-1 and CTLA-4, which have improved efficacy at the cost of higher toxicity.[13]

An attractive approach for local mAb delivery is the use of gene therapy vectors able to express mAbs inside the tumor mass. This approach has several potential advantages, such as: (1) mAb expression could be achieved with one single vector administration, avoiding repetitive injections of high doses of mAbs and lowering the price of treatment; (2) local mAb expression could increase mAb level and bioavailability in tumors, reducing systemic toxicity; and (3) the use of some types of viral vectors can induce damage or inflammation in the tumor, which could potentiate immune-stimulatory and antitumor effects. In fact, several preclinical and clinical studies have shown synergy between oncolytic viruses and immune checkpoint inhibitors.[14–16] Oncolytic viruses can induce antitumor effects by selectively destroying tumor cells, which also leads to the release of tumor antigens that can be taken up by APCs, thus promoting antitumor-specific T cell responses. In addition, viral infection can induce type I interferon (IFN-I) responses, which contributes to antitumor immunity and exerts synergistic effects with immunomodulatory mAbs.[17]

In the present study we have used two different viral vectors to deliver an anti-PD-L1 mAb locally in tumors. The Semliki Forest virus (SFV) vector contains as genome a positive-strand RNA able to self-replicate in infected cells, which can be engineered to express a transgene of interest.[18] SFV vectors expressing cytokines such as interleukin-12 (IL-12) have shown very potent antitumor properties in many preclinical studies because of high expression levels, induction of apoptosis in tumor cells, and stimulation of IFN-I responses.[19] However, recombinant SFV vectors enable transgene expression for only a short period of time because of their cytopathic and non-propagative nature. In contrast, adeno-associated virus (AAV)-derived vectors contain a single-strand DNA genome that can persist episomically in infected cells, providing very long-term transgene expression. AAV vectors have been successfully used in multiple clinical trials for the treatment of rare genetic diseases, such as hemophilia A and B or congenital Leber's amaurosis.[20,21] In fact, two AAV-derived vectors have been already approved for clinical use in humans.[22] In the present study we have compared side by side the antitumor efficacy of recombinant SFV and AAV vectors encoding the same anti-PD-L1 mAb in a colon adenocarcinoma model. Interestingly, local sustained expression of anti-PD-L1 from the AAV vector had very low antitumor efficacy, whereas short local mAb expression accompanied by IFN-I induction mediated by SFV was very effective and superior to therapies based on systemic or local mAb administration.

RESULTS

Development of AAV and SFV Vectors Expressing an Anti-PD-L1 mAb

We first determined the sequences of the variable regions of a hamster mAb raised against mouse PD-L1,[3] as described in the Supplemental Materials and Methods. Based on these sequences, we then generated AAV and SFV vectors expressing a chimeric hamster-mouse immunoglobulin G2a (IgG2a) against murine PD-L1 (see vector diagrams in Figure 1A). To verify the expression of the recombinant mAb, BHK cells were transfected with a plasmid containing the AAV vector (pAAV-aPDL1 [anti-PD-L1]) or infected with viral particles (VPs) generated with the SFV vector (SFV-aPDL1). The anti-PD-L1 mAb was detected in supernatants of cells transfected with pAAV-aPDL1 or infected with SFV-aPDL1 by western blot (Figure 1B). A PD-L1-specific binding ELISA was used to verify the capacity of recombinant anti-PD-L1 antibodies to bind PD-L1. This assay showed a very similar PD-L1 binding for the recombinant mAb expressed from AAV or SFV vectors (Figure 1C).

AAV and SFV Vectors Mediate Local Expression of Anti-PD-L1 mAb in Tumors

To confirm that viral vectors were able to express anti-PD-L1 mAb *in vivo*, they were injected intratumorally (i.t.) in C57BL/6 mice bearing subcutaneous MC38 colon adenocarcinoma tumor nodules. Mice received a single i.t. injection of 3×10^8 VPs of SFV-aPDL1 and 10^{11} VGs (viral genomes) of AAV-aPDL1. Other experimental groups included mice treated i.t. with 3×10^8 VPs of a SFV encoding the reporter gene β-galactosidase (SFV-LacZ) or with an equivalent volume of saline as negative control. Expression of anti-PD-L1 mAb was analyzed by PD-L1-specific binding ELISA in samples of serum and tumors obtained 1 and 5 days after vector injection. Both SFV-aPDL1 and AAV-aPDL1 expressed anti-PD-L1 mAb in tumors, reaching similar levels at day 1 (Figure 1D). These levels decreased at day 5 in the case of SFV-aPDL1, probably because of the cytopathic effect of this vector, whereas anti-PD-L1 mAb concentration remained significantly elevated for AAV-aPDL1 at day 5. mAb levels detected in serum with both vectors were very low at day 1, but increased at day 5 in mice treated with AAV-aPDL1, whereas they were almost undetectable in animals that had received SFV-aPDL1 (Figure 1E). As expected, no mAb expression was observed in the SFV-LacZ and saline groups.

SFV-aPDL1 Elicits Higher Antitumor Effects Than AAV-aPDL1 against Colon Adenocarcinoma Tumors

To evaluate the antitumor potential of SFV and AAV vectors expressing antiPD-L1 mAb, mice bearing subcutaneous MC38 tumors with an average diameter of 3–3.5 mm were treated with a single i.t. injection of 3×10^8 VPs of SFV-aPDL1 or 10^{11} VGs of AAV-aPDL1, because these doses had shown to provide similar mAb expression in tumors (Figure 1D). As controls, tumor-bearing mice were treated with either 3×10^8 VPs of SFV-LacZ or an equivalent volume of saline. In parallel, additional groups of mice were treated with three doses of SFV-aPDL1 or SFV-LacZ (3×10^8 VPs each), administered every 48 h to determine whether the antitumor effect of this short-term expression vector could be enhanced by repeated administrations. The efficacy of treatment was evaluated by measuring tumor size every 3–4 days (Figure 2A) and monitoring survival in each group (Figure 2B). SFV-aPDL1 showed a clear antitumor effect that resulted in significant control of tumor growth, leading to complete remissions

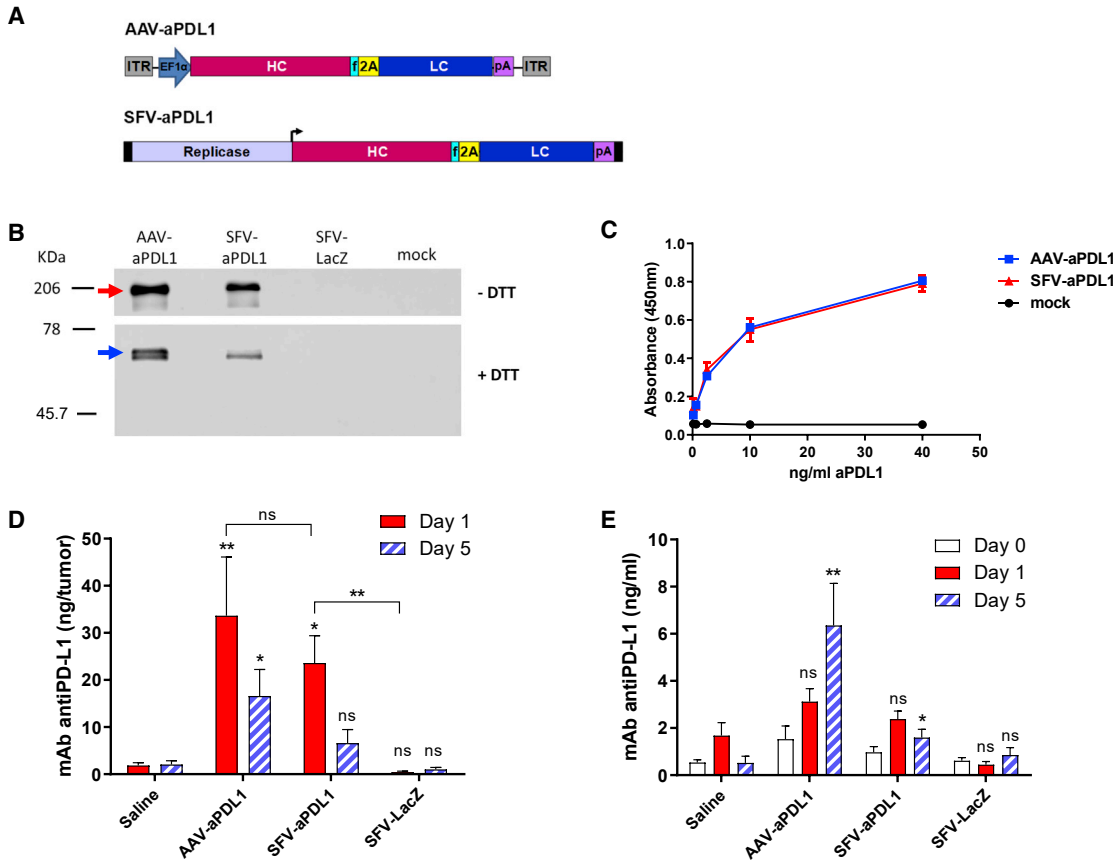

Figure 1. AAV and SFV Viral Vectors Express Anti-PD-L1 mAb in Cultured Cells and in Tumors *In Vivo*

(A) Schematic representation of AAV and SFV vectors expressing anti-PD-L1 mAb. In SFV-aPDL1, black rectangles at the ends represent 5′ and 3′ viral sequences necessary for replication, and the black arrow represents the SFV subgenomic promoter (the replicase gene is not to scale). (B and C) BHK cells were transfected with AAV-aPDL1 plasmid or infected with the indicated SFV vectors, or mock infected, and the supernatants were collected 48 h later and analyzed as indicated. (B) Western blot was performed under non-reducing (−DTT) or reducing (+DTT) conditions using an anti-mouse IgG peroxidase-conjugated antibody. Red and blue arrows show the complete mAb and the HC of anti-PD-L1 mAb, respectively (LC could not be detected due to low affinity of secondary antibody for lambda LC). (C) A PD-L1-binding ELISA was performed by coating ELISA plates with recombinant PD-L1-Fc and incubating them with serial dilutions of supernatants from cells transfected or infected with the indicated vectors. In order to compare binding of anti-PD-L1 mAb expressed by both vectors, we previously quantified IgG in each sample (using a total mouse IgG ELISA kit) and adjusted mAb concentrations to 40 ng/mL, from which 1:4 dilutions were tested. For the mock-infected sample, the first dilution was prepared with a volume equivalent to the one used for the sample with lower mAb concentration. (D and E) C57BL/6 mice bearing subcutaneous MC38 tumors having an average diameter of 5.5 mm received a single intratumoral dose of 10^{11} VGs (AAV-aPD-L1), 3×10^{8} VPs (SFV-aPD-L1 and SFV-LacZ), or the same volume of saline. The amount of recombinant anti-PD-L1 mAb present in tumor extracts (D) and serum (E) was determined at the indicated times using a PD-L1-binding ELISA (n = 5 for each time point). Asterisks above bars indicate comparison of each group with saline. *p < 0.05; **p < 0.01. One representative experiment out of two performed is shown. 2A, foot-and-mouth disease virus 2A autoprotease; EF1α, human elongation factor 1α promoter; f, furine protease cleavage site; HC, mAb heavy chains; ITR, AAV inverted terminal repeats; LC, mAb light chains; ns, not significant; pA, synthetic polyadenylation sequence. Data represent the mean + SEM.

in 43% of tumors, compared with only 14% in the case of AAV-aPDL1. In fact, this last vector did not show a significant effect on tumor reduction when compared with the saline control group. On the other hand, the antitumor effect of SFV-aPDL1 slightly improved when three doses of vector were administered, reaching 57% of complete remissions, although survival was not significantly increased. All animals that rejected tumors remained tumor-free for the rest of the experiment (>2–3 months). Interestingly, SFV-LacZ showed a low antitumor effect that increased when mice received three doses of vector, possibly because of the induction of apoptosis and IFN-I responses induced by SFV, as will be discussed later. However, the antitumor effect provided by this control SFV vector was significantly lower than the one obtained with SFV-aPD-L1 (Figures 2A and 2B).

In order to determine whether treatment with vectors expressing anti-PD-L1 mAb induced immunological memory, mice that had rejected tumors after SFV-aPDL1 treatment were rechallenged subcutaneously with MC38 cells. No development of tumors was observed in cured animals, in contrast with naive controls, indicating that the vector had induced immunological memory, which could protect against

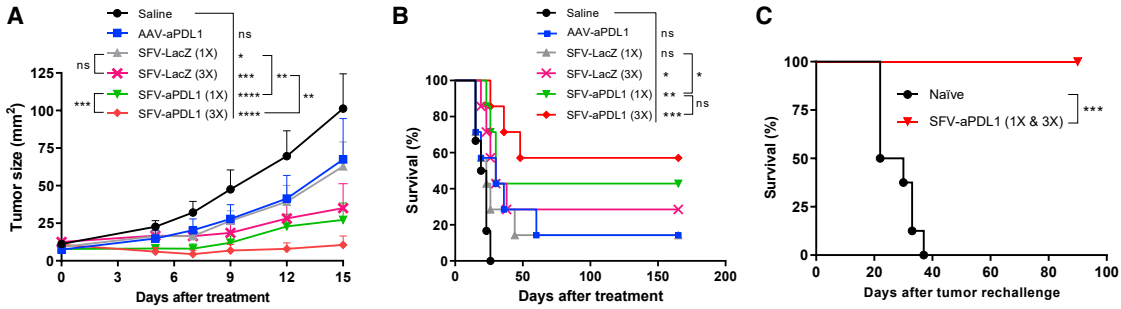

Figure 2. Evaluation of Antitumor Efficacy of AAV and SFV Viral Vectors Expressing Anti-PD-L1 mAb in MC38 Subcutaneous Tumors

A total of 5×10^5 MC38 cells were inoculated subcutaneously into the right flank of C57BL/6 mice and approximately 7 days later (day 0), when the average diameter was 3–3.5 mm, animals received one intratumoral dose of 10^8 VGs of AAV-aPDL1 or 3×10^8 VPs of SFV-aPDL1or SFV-LacZ (1×). A control group received the same volume of saline. Two additional groups received three intratumoral doses of SFV-aPDL1 or SFV-LacZ given on days 0, 2, and 4 (3×). (A) Evolution of tumor size. Data represent the mean tumor size (mm^2) + SEM. (B) Survival after treatment. (C) Survival after tumor rechallenge. Mice treated with SFV-aPDL1 (1× or 3×) that rejected tumors (n = 7) were rechallenged 2–3 months later with 5×10^5 MC38 cells, and survival was analyzed using naive mice that received the same amount of tumor cells as controls (n = 8). For (A) and (B), one representative experiment (n = 7) out of three performed is shown (in B the statistical analysis was performed using pooled data from two independent experiments). *p < 0.05; **p < 0.01; ***p < 0.001; ****p < 0.0001. ns, not significant.

possible recurrences (Figure 2C). We also determined whether treatment with SFV-aPDL1 could induce abscopal effects in non-treated nodules. Mice receiving SFV-aPDL1 in one tumor showed a significant reduction of tumor size both in treated and in non-treated nodules (Figure S1A), indicating that this kind of therapy can induce abscopal effects. We also observed significantly higher survival in SFV-aPDL1-treated mice (Figure S1B), although long-term survival was not reached, most likely because the abscopal effect was not potent enough to eliminate non-treated tumors.

To investigate whether SFV-aPDL1 also had antitumor efficacy in other types of tumors, we proceeded to test it in a melanoma model that is particularly resistant to PD-L1 blockade, such as B16-ovalbumin (OVA) tumors derived from the B16F10 melanoma cell line.[23] For this purpose, C57BL/6 mice carrying subcutaneous B16-OVA tumors were injected i.t. with a single dose of SFV-aPDL1 (3×10^8 VPs). As control groups, we included mice in which tumors were treated with the same dose of SFV-LacZ or saline (mock-treated group). SFV-aPDL1 showed clear antitumor efficacy that resulted in a significant delay of tumor growth after the injection of the virus (Figures S2A and S2B). The SFV-aPDL1 vector also increased significantly the survival of treated animals compared with saline or SFV-LacZ (Figure S2C).

SFV-Mediated Local Expression of Anti-PD-L1 mAb Induced Higher Antitumor Effects Than Systemic or Local Administration of the Same mAb

To evaluate whether local expression of anti-PDL1 mAb by SFV could be an alternative to the administration of the same mAb as recombinant protein, we carried out a comparative study of these two strategies. For this purpose, mice bearing MC38 subcutaneous tumors were treated with a single i.t. injection of SFV-aPDL1 (3×10^8 VPs) or received anti-PD-L1 mAb either i.t. or intraperitoneally (i.p.). For the i.t. route, we used two doses of 100 ng mAb given with a 48-h interval, each dose being approximately 5-fold higher than the amount expressed by SFV-aPDL1 in the tumor as determined in Figure 1D. For the i.p. route, we used a standard mAb dosing (three doses of 100 μg given every 72 h). SFV-aPDL1 was clearly more potent than anti-PD-L1 mAb given i.t. (Figures 3A–3C). In the case of anti-PD-L1 mAb given i.p., it was able to provide a reduction in tumor growth that was less potent than SFV-aPDL1, but this last vector provided a significantly higher survival (Figure 3C). These results suggest that SFV-mediated local inflammation in combination with anti-PD-L1 expression is responsible for the higher antitumor effect of this vector. To test this hypothesis, we evaluated the antitumor efficacy of SFV-LacZ given i.t. in combination with anti-PD-L1 mAb delivered i.p. This combination therapy induced a significant reduction in tumor growth with 25% complete regressions, whereas no regressions were observed with each single agent (Figures S3A and S3B). In addition, combination therapy significantly increased survival, in contrast with each single agent (Figure S3C).

SFV-aPDL1 Induces Type I IFN Responses Locally in Tumors

As shown before, SFV-aPDL1 was more potent than AAV-aPDL1 at inducing antitumor responses (Figure 2), despite the fact that the AAV vector expressed the antiPD-L1 mAb at similar levels and for a longer time (Figure 1D). One possible mechanism to explain the higher antitumor effect of SFV-aPDL1 could be related to the fact that SFV RNA replication can induce IFN-I responses locally in the tumor, which have been described to potentiate checkpoint inhibitors' antitumor effects.[17] To evaluate this possibility, we analyzed the induction of IFN-stimulated genes (ISGs) in mice bearing MC38 tumors that were injected i.t.with the following vectors: SFV-aPDL1, SFV-LacZ (3×10^8 VPs), or AAV-aPDL1 (10^{11} VGs). Tumors were processed 17 h after treatment and analyzed by qRT-PCR with primers specific for ISGs, including 2′-5′-oligoadenylate synthetase 2 (OAS2), Mx1, TRIM, and STAT1, as well as for SFV replicase (Figure 4). Notably, the level of ISGs was significantly upregulated in tumors treated with SFV vectors compared with those that received AAV-aPDL1 or saline,

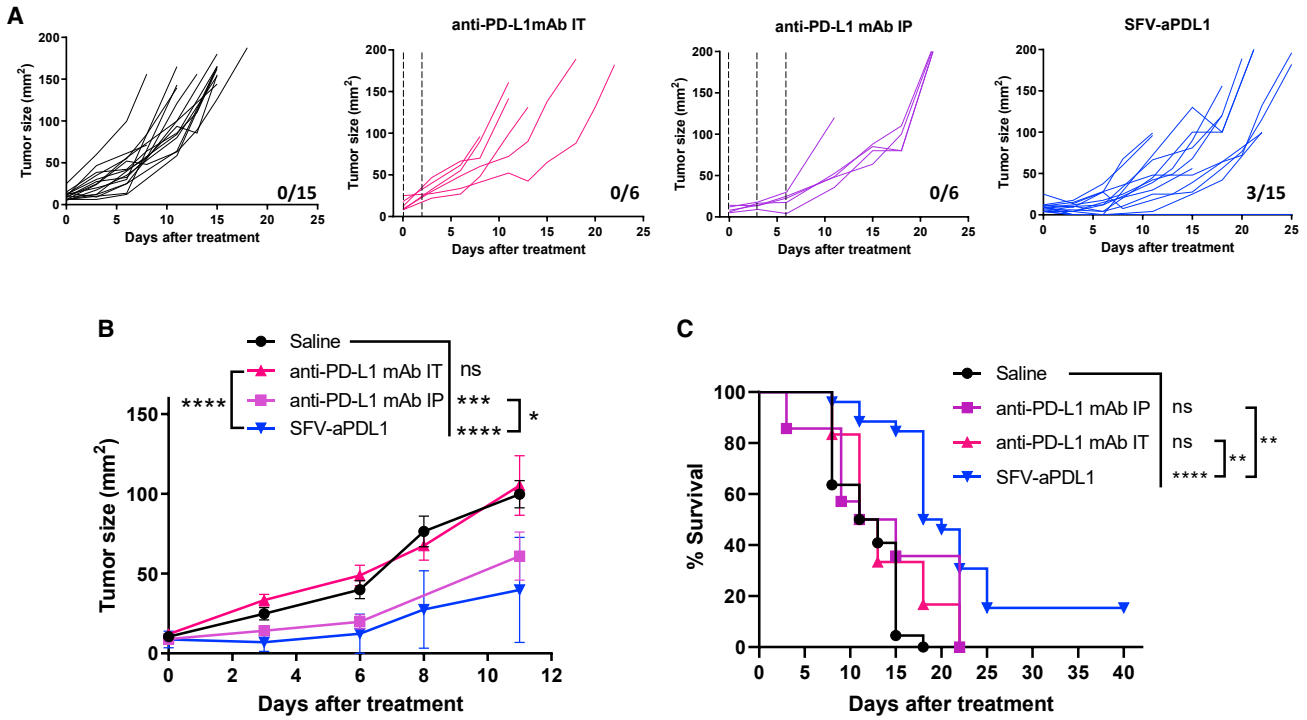

Figure 3. SFV-aPDL1 Given Intratumorally Showed Greater Antitumor Effect Than Anti-PDL1 mAb Administered Locally or Systemically

C57BL/6 mice bearing subcutaneous tumors were inoculated intratumorally with a single dose of SFV-aPDL1 (3×10^8 VPs), as described in Figure 2. In parallel, mice with similar tumors received three intraperitoneal (i.p.) doses of 100 μg of anti-PDL1 mAb on days 0, 3, and 6, or two intratumoral (i.t.) doses of 100 ng of anti-PDL1 mAb on days 0 and 2. Mice treated with saline were used as negative control. (A) Evolution of tumor size (mm^2) along time for each individual mouse. The fractions in the right lower corner of each graph indicate the number of complete regressions/total number of mice in each group. Dashed lines indicate the times of mAb administrations. (B) Mean tumor size evolution ± SEM. (C) Survival after treatment (pooled data from two independent experiments). *$p < 0.05$; **$p < 0.01$; ***$p < 0.001$; ****$p < 0.0001$. One representative experiment out of two performed is shown. ns, not significant.

confirming the induction of IFN-I responses by SFV. The detection of high levels of viral RNA in SFV-treated tumors confirmed the local replication of these vectors (Figure 4).

Analysis of PD-L1 Expression in Tumors

The higher antitumor effects mediated by SFV-aPDL1 in comparison with SFV-LacZ are likely mediated by PD-L1 blocking on tumor cells. We confirmed that both MC38 and B16-OVA cells were able to express PD-L1 *in vitro*. As shown in Figure S4A, both tumor cell lines showed basal PD-L1 levels that significantly increased when incubated with IFN-gamma, with a higher increase in B16-OVA. We also confirmed that both types of cells expressed PD-L1 in tumors implanted *in vivo* (Figure S4B). Interestingly, treatment with SFV vectors significantly increased PD-L1 in B16-OVA tumors, which could be mediated by the induction of IFN-I responses. This effect was not observed in MC38 tumors, suggesting that upregulation of PD-L1 in these cells is less potent.

SFV-aPDL1 Induces Potent Cellular Immune Responses with Elevation of Co-stimulatory and Co-inhibitory Molecules

In order to characterize immune responses induced by SFV-aPDL1, mice bearing MC38 tumors received by i.t. injection 3×10^8 VPs of this vector. Animals were sacrificed 5 days later, and immune cell subpopulations from tumors, tumor draining lymph nodes (TDLNs), and peripheral blood were analyzed by multicolor flow cytometry analysis. As control for this study, we used mice injected with the same dose of SFV-LacZ or with an equivalent volume of saline solution. We also included a group of mice inoculated with AAV-aPDL1 as an additional control. The fact that this vector expressed levels of anti-PD-L1 mAb similar to SFV-aPDL1, but induced only marginal antitumor effects could provide information about the immunological changes mediated by the mAb.

SFV-aPDL1 was able to significantly increase total CD8 T cells in tumors, TDLNs, and peripheral blood (Figures 5A–5C, left graphs). Total CD4 T cells were also increased by SFV-aPDL1, reaching significance in TDLNs and blood (Figures 5A–5C, right graphs). Interestingly, tumor-specific CD8 cells, which were measured using MHC class I tetramers specific for a MC38 dominant epitope (tumor-associated KSPWFTTL peptide [KSP]), were more elevated in tumors and TDLNs from SFV-aPDL1-treated mice, suggesting that this vector was inducing a more potent local response. Tumor-specific CD8 cells were also detected in blood in SFV-treated mice (Figure 5C, central graph). In order to determine whether tumor CD8 cells had an effector capacity, we analyzed the

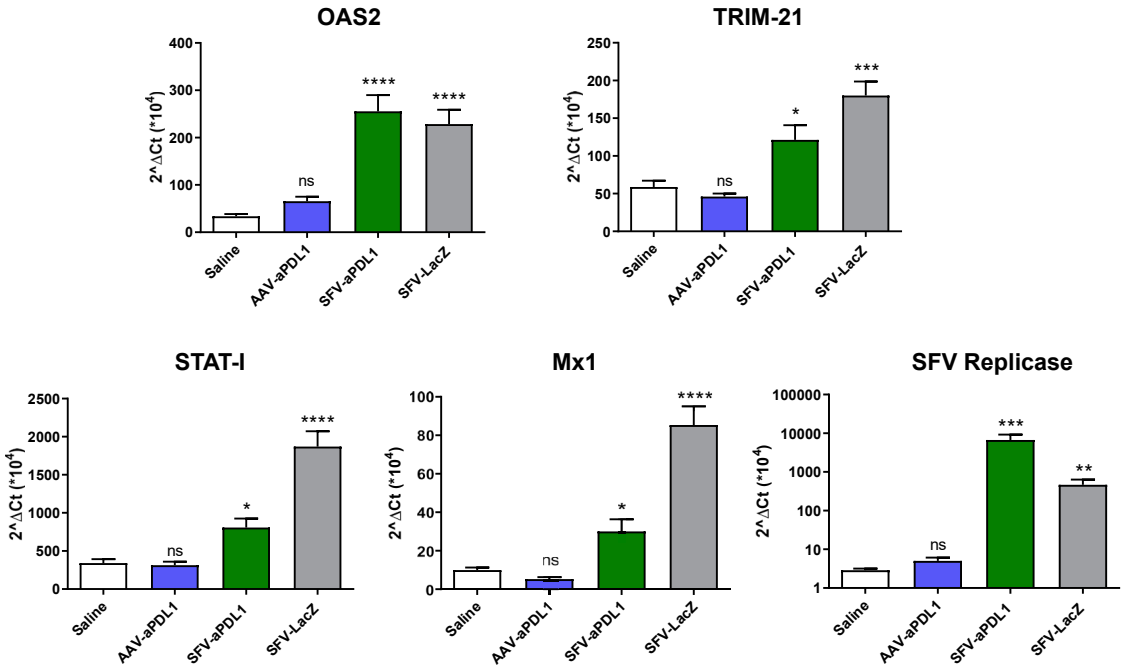

Figure 4. Analysis of the Expression of Genes Induced by Type I IFN in MC38 Subcutaneous Tumors

C57BL/6 mice bearing subcutaneous MC38 tumors received a single intratumoral dose of 3×10^8 VPs (SFV-aPD-L1 and SFV-LacZ), 10^{11} VGs (AAV-aPD-L1), or the same volume of saline. Tumor samples were extracted and processed 17 h after treatment as described in the Materials and Methods. Finally, they were analyzed by qRT-PCR with primers specific for the indicated genes. Asterisks above each bar indicate the statistical comparison of each group with the saline group. *$p < 0.05$; **$p < 0.01$; ***$p < 0.001$; ****$p < 0.0001$. ns, not significant. Data represent the mean + SEM.

expression of the CD62L surface marker, whose downregulation was associated with the acquisition of an effector-like phenotype. As observed in Figure S5A, both total and KSP-specific CD8 tumor cells from SFV-aPDL1-treated mice had a significantly lower level of CD62L compared with all of the other groups.

We then proceeded to analyze the percentage of CD8 and CD4 tumor-infiltrating T cells (TILs) expressing co-stimulatory (CD137, OX40, and inducible T cell costimulator [ICOS]) and co-inhibitory (PD-1, LAG-3, 2B4, and TIM-3) molecules. Interestingly, the percentage of CD137- and OX40-positive CD8 TILs was increased in mice treated with SFV vectors, with no significant differences observed between SFV-aPDL1 and SFV-LacZ (Figure 6A). This trend was also observed in KSP-specific CD8 TILs for both markers, although it did not reach significance. No significant differences were observed for ICOS (Figure S6). Regarding co-inhibitory markers, an increase of LAG-3 was detected in total CD8 TILs from mice treated with SFV vectors (Figure 6B). Despite its lack of antitumor efficacy, AAV-aPDL1 seemed to diminish LAG3 in CD8 cells. No relevant changes in the expression of PD-1, 2B4, and TIM-3 in CD8 TILs were observed between groups (Figure 6B; Figure S6). Regarding CD4 TILs, we observed a significant downregulation of PD-1 and TIM-3 in SFV-treated mice (Figure 6B; Figure S6). All together, these results suggest that in contrast with AAV-aPDL1, SFV-aPDL1 was able to promote tumor infiltration by T cells, increasing the number of tumor-specific CD8 cells with an effector phenotype. Changes in co-stimulatory and co-inhibitory markers were similar between SFV-aPDL1 and SFV-LacZ, suggesting that they were probably due to the self-replication nature of the SFV RNA vector, which is able to promote inflammation and IFN-I responses by itself as shown before (Figure 4).[24]

In order to determine whether SFV-aPDL1 was inducing similar changes in B16-OVA, we analyzed immunological markers in TILs from these tumors. In this case, we observed a significant upregulation of both total and tumor-specific CD8 cells in mice treated with SFV-aPDL1, in contrast with those treated with SFV-LacZ or saline, confirming the results observed in MC38 (Figure 7). A lower level of CD62L was also observed in CD8 cells from SFV-aPDL1-treated tumors, suggesting an effector-like phenotype (Figure S5B). In addition, both SFV-aPDL1 and SFV-LacZ induced a reduction of PD-1 in tumor-specific CD8 cells, although it reached significance only with this last vector (Figure S7A). However, in contrast with MC38, no relevant changes were observed in LAG-3 and CD137 (Figures S7B and S7C), indicating tumor-inherent differences despite the fact that both models responded to treatment.

Intratumoral Injection of SFV-aPDL1 Synergizes with Systemic CD137 Co-stimulation, But Not with LAG-3 Inhibition

The upregulation of some co-stimulatory (CD137 and OX40) and co-inhibitory (LAG-3) receptors in tumor CD8 cells induced by

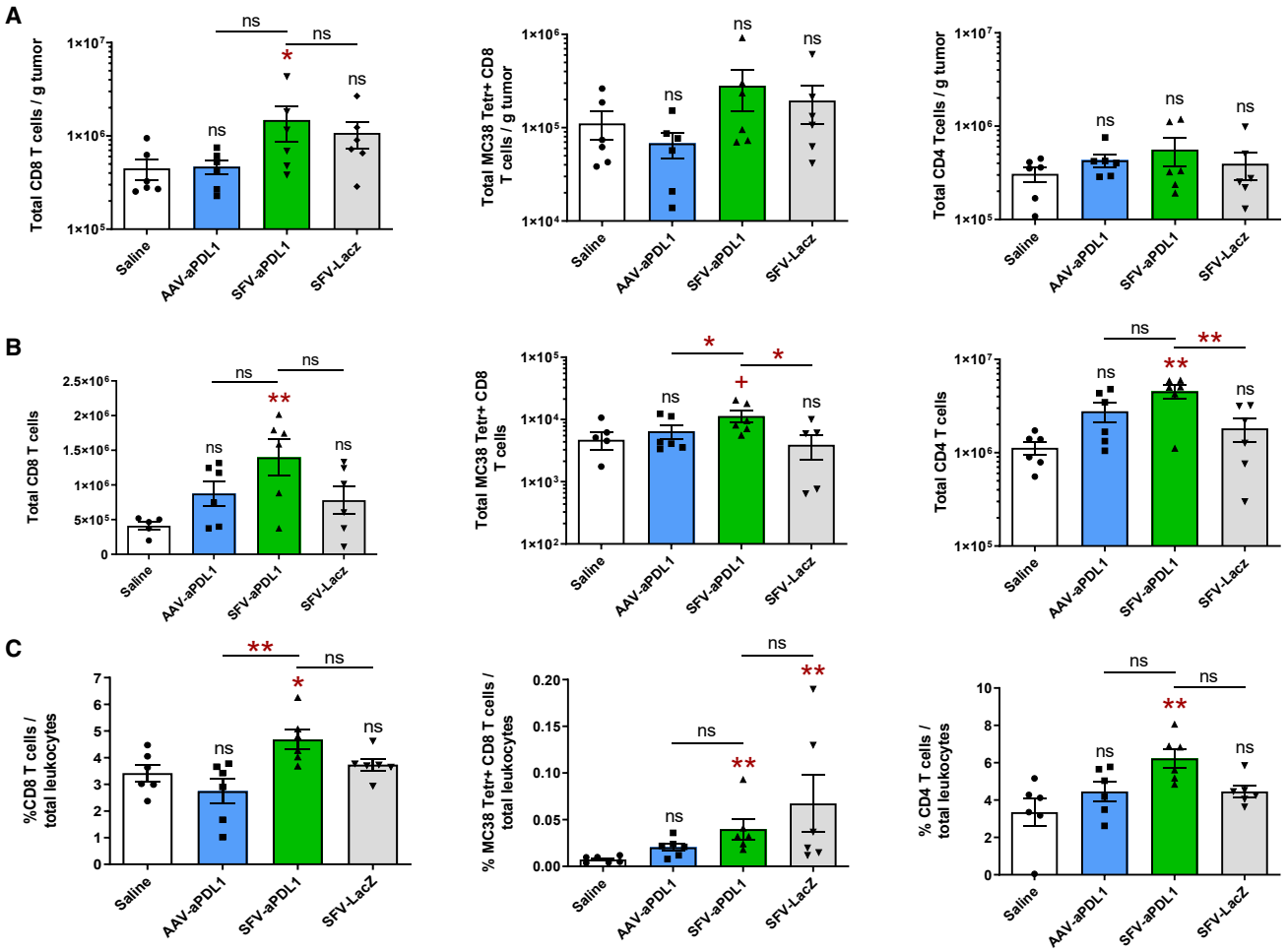

Figure 5. Analyses of CD8 and CD4 T Cells in MC38 Tumors, Lymph Nodes, and Blood

C57BL/6 mice bearing subcutaneous MC38 tumors were inoculated with the indicated vectors or saline as described in Figure 1D. Five days after the administration of vectors, tumors and tumor draining lymph nodes (TDLNs) were excised and digested, and single-cell suspensions were analyzed by flow cytometry. Blood was collected on the same day and analyzed by flow cytometry. Data represent the mean (n = 6) ± SEM of total CD8 (left graphs), tumor-specific CD8 (MC38 Tetr$^+$, central graphs), and CD4 T cells (right graphs) in tumors (A), TDLNs (B), and blood (C). Gating strategies are shown in Figure S9. Asterisks above each bar indicate the statistical comparison of each group with the control saline group. Other comparisons are indicated by horizontal bars. $^+p < 0.1$; $^*p < 0.05$; $^{**}p < 0.01$. ns, not significant.

SFV-aPDL1 suggested that this therapy could benefit from a combination with mAbs able to stimulate or block these receptors, respectively. To test our hypothesis, we treated mice bearing MC38 subcutaneous tumors with 3×10^8 VPs of SFV-aPDL1 given i.t. combined with either anti-CD137 or anti-LAG-3 mAbs given i.p. In this case we used tumors slightly larger than in previous experiments (4–5 mm of average diameter) in order to increase our therapeutic window. Control groups received only mAbs, only the vector, or saline. Despite the upregulation of LAG-3 induced by SFV vectors, combination with anti-LAG-3 mAb contributed only slightly to reducing the progression of tumors (Figure 8). The anti-LAG-3 single treatment did not have any therapeutic effect in this model as had been previously described.[25] However, combination of i.t. SFV-aPDL1 and systemic anti-CD137 mAb showed a very potent antitumor effect that resulted in elimination of 50% of tumors with long-term survival (Figure 8). In contrast, SFV-aPDL1 or anti-CD137 mAb given as single agents were able to induce only 25% and 11% of complete regressions, respectively. It has been previously reported that resistance to anti-CD137 therapy can be overcome by PD-1/PD-L1 blockade.[26] To determine whether anti-CD137 target cells could be affected by this blockade in our model, we analyzed TILs from MC38 tumors, observing that almost 100% of CD137-positive CD8 cells were also positive for PD-1 (Figure S8). This could partially explain the beneficial effects of co-stimulation via CD137 and simultaneous relief from PD-1 inhibition using SFV-aPDL1, as observed in this study.

DISCUSSION

In this study we evaluated the antitumor efficacy of AAV and SFV viral vectors able to express an anti-PD-L1 mAb locally in tumors. We chose these vectors because of the fact that both have attractive

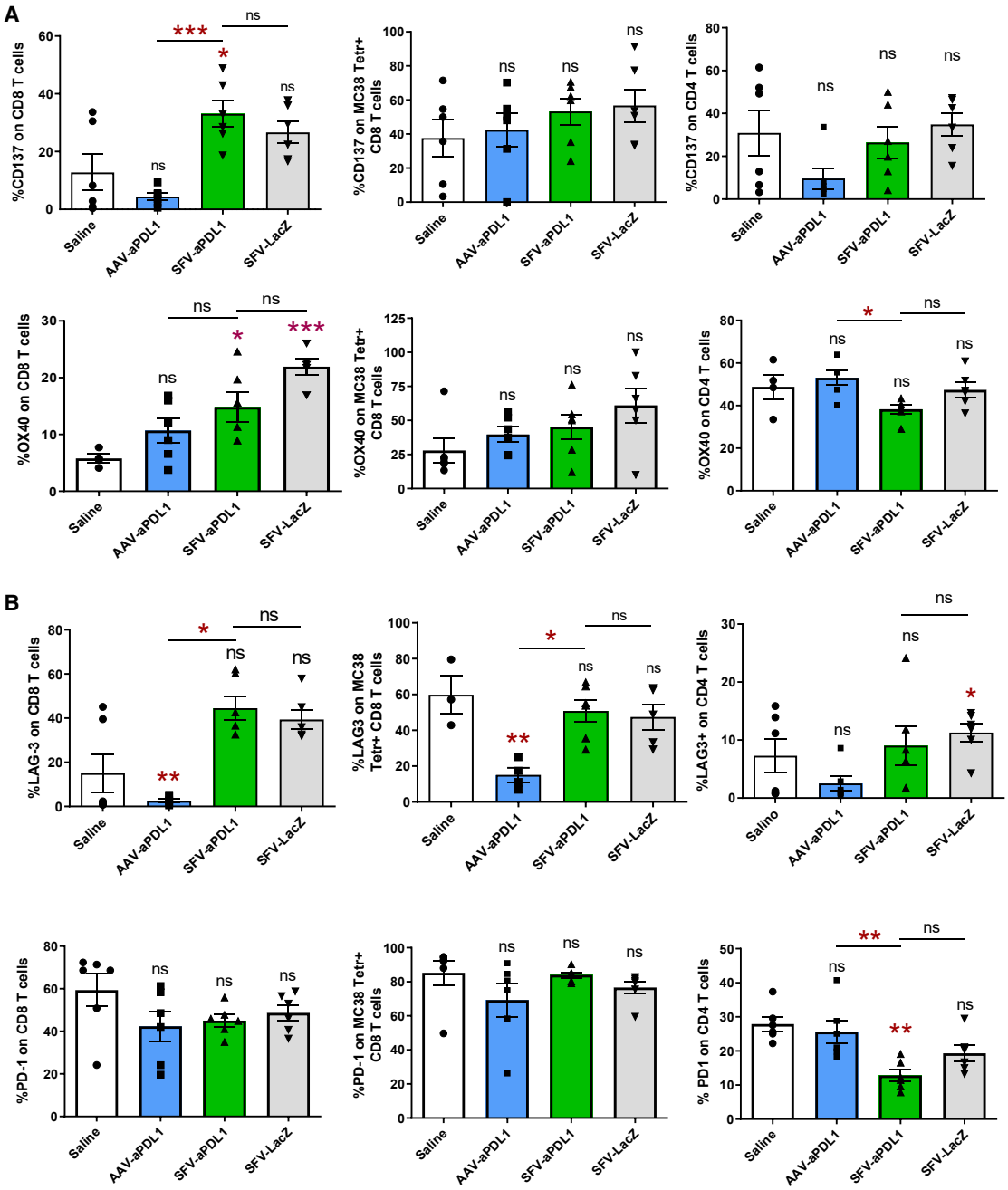

Figure 6. Analyses of Co-stimulatory and Co-inhibitory Immunological Markers on MC38 Tumor T Cells

Tumor-infiltrating lymphocytes obtained as described in Figure 5 were analyzed by flow cytometry with antibodies specific for the immunological co-stimulatory markers CD137 and OX40 (A) and for immunological co-inhibitory markers PD-1 and LAG3 (B). Data show levels (mean ± SEM, n = 6) of each marker in total CD8 T cells (left graphs), tumor-specific CD8 T cells (MC38 Tetr$^+$, central graphs), and total CD4 T cells (right graphs). Asterisks above each bar indicate the statistical comparison of each group with the control saline group. Other comparisons are indicated by horizontal bars. *$p < 0.05$; **$p < 0.01$; ***$p < 0.001$. ns, not significant.

properties for cancer immunotherapy. AAV is a single-strand DNA vector that is easy to produce at high scale and has been extensively used in human patients without showing toxicity.[27] The main advantage of this vector is the fact that it can provide long-term expression of the desired transgene, which might be required to sustain appropriate levels of immunomodulatory mAbs inside tumors. AAV vectors have also been successfully used for cancer immunotherapy in preclinical models by expressing antitumoral cytokines, such as

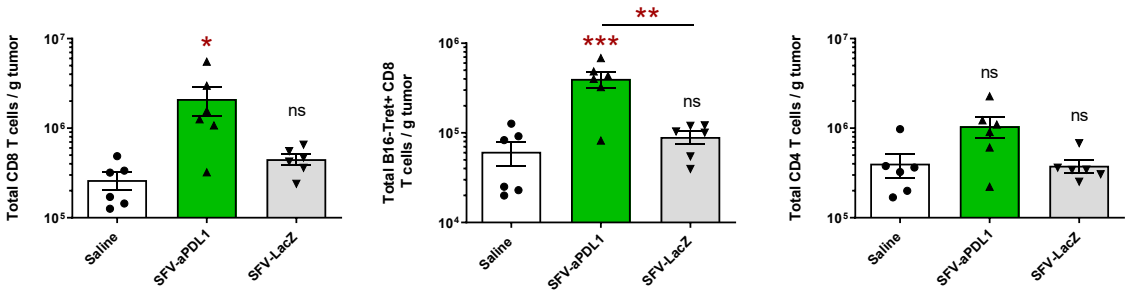

Figure 7. Analyses of CD8 and CD4 T Cells in B16-OVA Tumors

A total of 5×10^5 B16/OVA cells were inoculated subcutaneously into the right flank of C57BL/6 mice and 6 days later, when tumors had an average diameter of 4–5 mm, animals received one intratumoral dose of 3×10^8 VPs of the indicated SFV-derived vectors or an equivalent volume of saline. Five days after the administration of vectors, tumors were excised, digested, and single-cell suspensions were analyzed by flow cytometry. Data represent the mean (n = 6) ± SEM of total CD8 (left graphs), tumor-specific CD8 (B16-Tetr$^+$, central graphs), and CD4 T cells (right graphs) in tumors. Asterisks above each bar indicate the statistical comparison of each group with the control saline group. Other comparisons are indicated by horizontal bars. *$p < 0.05$; **$p < 0.01$; ***$p < 0.001$. ns, not significant.

IL-12[28] or IL-27.[29] SFV is an RNA vector that can replicate in infected cells, leading to very high expression levels of desired transgenes.[18] In contrast with AAV, SFV vectors can provide only a very short transgene expression, due to the fact that they are unable to propagate and induce apoptosis in infected cells. Despite short expression, SFV vectors expressing IL-12,[30] IFNα,[31] or a combination of the dendritic cell differentiation factor Flt3L and chemokine XCL1[32] have shown potent antitumor effects against a variety of preclinical models, including spontaneous tumors in the case of SFV-IL-12.[33,34] One of the key mechanisms by which SFV can exert its antitumor action is based on the potent induction of IFN-I responses in infected cells. In fact, we have shown that IFN-I induction is strictly required for the therapeutic effects of SFV-IL-12 and is dependent on IPS-1 and Trif signaling and independent of the Myd88 pathway.[24] Given that previous studies had shown that the antitumor effect of immunomodulatory mAbs could be highly potentiated with agents able to induce IFN-I responses, such as polyinosinic:polycytidylic acid (poly(I:C)) or oncolytic viruses,[17,35,36] we reasoned that an SFV vector able to express an anti-PD-L1 mAb could combine both properties in a single agent. In addition, because it has been shown that IFNα and IFNβ can induce PD-L1 expression in tumor cells,[17] "arming" an IFN-I-inducing vector with an anti-PD-L1 mAb could enhance its antitumor potential. One drawback of this strategy could be that the anti-PD-L1 mAb will be expressed transiently in the tumor, as we observed in mice treated with SFV-aPDL1, in which expression was not detected after 24 h (Figure 1D). In contrast, mice that received AAV-aPDL1 were able to express the mAb during at least 5 days. However, despite the much shorter, but quantitatively similar, mAb expression of SFV-aPDL1, this vector was able to induce more potent antitumor effects than AAV-aPDL1 in the MC38 colon adenocarcinoma model (Figure 2).

The effect of SFV-aPDL1 was slightly improved by providing three doses of the vector given every 48 h, in an attempt to maintain anti-PD-L1 levels in the tumor for longer times. In agreement with this result, we had previously observed that the antitumor effects of SFV-IL-12 could also be improved with repetitive administrations of the vector.[37] SFV-aPDL1 was also able to inhibit the growth of B16-OVA tumors, although in this case the antitumor effect was transient in most mice, resulting in 11% complete regressions. B16-OVA tumors have shown in previous studies to be more resistant to therapies based on SFV vectors compared with MC38.[38] In addition, several studies performed by us and others have shown that mAbs able to block the PD-1/PD-L1 axis are not very efficient in this tumor model, which could explain the lower efficacy of SFV-aPDL1.[39] Interestingly, SFV vectors induced higher PD-L1 expression in B16-OVA tumor cells compared with MC38 (Figure S4), which could explain in part why SFV therapy was less potent in B16-OVA, because higher amounts of antiPD-L1 are probably needed in this model to overcome this resistance mechanism.

Comparison of local SFV-aPDL1-based therapy with systemic administration of anti-PD-L1 mAb was important to demonstrate that local mAb delivery could reach the same or slightly higher therapeutic effects, as it was the case (Figure 3). It is important to note that, as observed in mice treated with AAV-aPDL1, i.t. delivery of the anti-PD-L1 mAb without the inflammation induced by SFV had negligible antitumor effects. In fact, by combining local SFV-LacZ administration and systemic anti-PDL1 mAb, we observed higher antitumor effects than with each separated agent (Figure S3).

In order to get some insights on the mechanisms by which SFV-aPDL1 provided stronger antitumor responses than AAV-PDL1, we analyzed the tumor microenvironment of treated mice at two levels, namely, the analysis of IFN-I responses and the characterization of immune cells; these were also analyzed both in blood and in TDLNs. As expected, SFV-aPDL1, and also control vector SFV-LacZ, were able to significantly upregulate different ISGs, which included Mx1, OAS-2, TRIM-21, and STAT-I (Figure 4). However, AAV-aPDL1 did not change the expression of any of these genes, being unable to benefit from IFN-I responses. The induction of an IFN-I response by SFV is most likely due to its RNA replication in infected cells, as has been previously reported.[24]

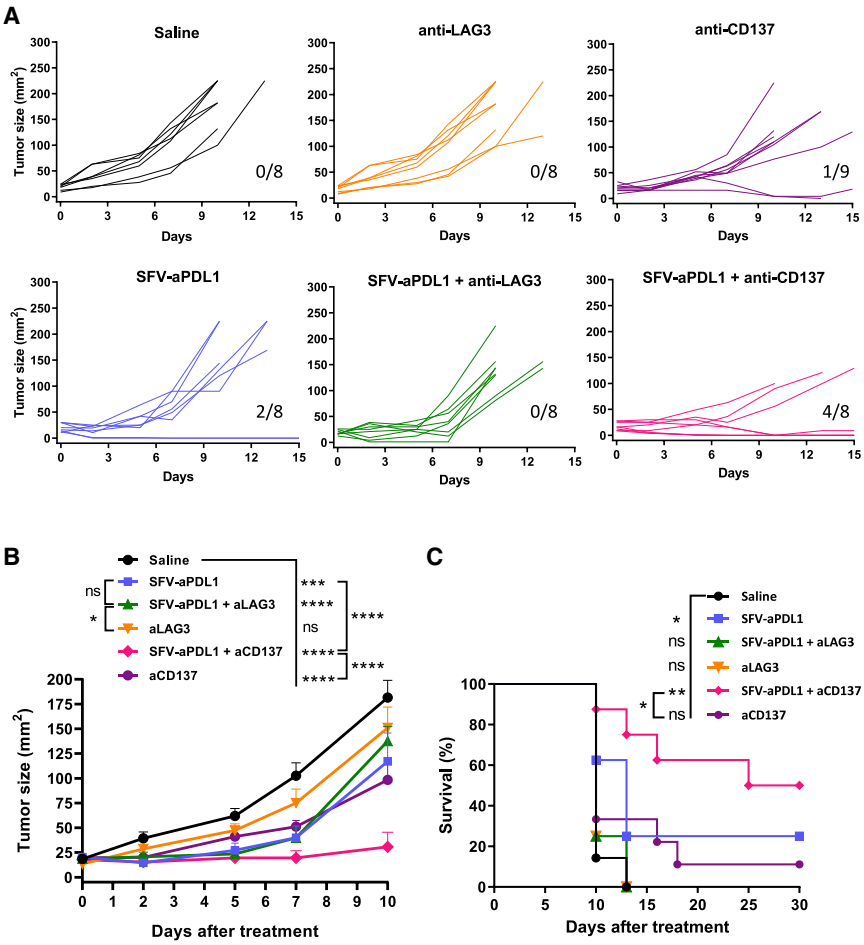

Figure 8. Treatment Efficacy of SFV-aPDL1 in Combination with Anti-CD137 and Anti-LAG3 mAbs

Mice bearing subcutaneous MC38 tumors (4–5 mm of average diameter) were inoculated with one intratumoral dose of SFV-aPDL1 (3×10^8 VPs) or saline (day 0). Then, one third of mice were intraperitoneally injected with anti-CD137 (days 0 and 6) or with anti-LAG3 (days 3, 6, and 9). (A) Graphs show the evolution of tumor size over time for each individual mouse. The fractions in the right lower corner of each graph indicate the number of complete regressions/total number of mice for each group. (B) Data represent the mean tumor size for all groups + SEM (n = 8–9). (C) Survival after treatment. *p < 0.05; **p < 0.01; ***p < 0.001; ****p < 0.0001. One representative experiment out of two performed is shown. ns, not significant.

Regarding immunological changes, a significantly higher infiltration of tumor-specific CD8 cells with effector phenotype was observed in MC38 tumors receiving SFV-aPDL1, but not in those treated with AAV-aPD-L1 or control SFV-LacZ vector (Figure 5; Figure S5). A similar effect was also observed in B16-OVA tumors (Figure 7), suggesting that to unleash potent immune responses, both expression of anti-PD-L1 mAb and induction of IFN-I responses were required. Interestingly, in MC38 tumors, SFV-aPDL1 and SFV-LacZ upregulated several co-stimulatory and co-inhibitory receptors in tumor CD8-infiltrating cells to similar levels, suggesting that these changes are mediated by the induction of IFN-I responses or by other mechanisms related to SFV infection per se. These last changes provided clues for possible combinatorial treatments. In the present work we tested the combination of local injection of SFV-aPDL1 with systemic administration of either anti-CD137 or anti-LAG-3 mAbs. Unexpectedly, anti-LAG-3 mAb was unable to enhance the antitumor activity of SFV-aPDL1. This is in contrast with other studies where a combination of anti-PD-1 and anti-LAG-3 mAbs was highly synergistic against MC38 tumors.[25] Although we do not have a clear explanation for the lack of synergy in our model, it is possible that higher levels of anti-PD-L1 than the ones provided locally by our vector were required for this effect. Finally, we were able to observe an enhancement of the antitumor response by combining SFV-aPDL1 and anti-CD137 mAb. Synergy between anti-PD-L1 and anti-CD137 mAbs had been previously reported and is probably due to the concomitant stimulation of anti-CD137 on activated CD8 T cells and the inhibition of the interaction of these cells with PD-L1 on tumor cells.[40] In fact, we observed that almost the totality of $CD137^+$ CD8 TILs from MC38 tumors also expressed PD-1 on their surface (Figure S8), suggesting that anti-CD137 therapy could benefit from PD-1/PD-L1 blockade, as shown previously by Hirano and colleagues.[26] Given the toxicity reported by anti-CD137 agonist mAbs in clinical trials,[41] it would be highly interesting to evaluate the possibility to also express this mAb locally in tumors from SFV vectors.

Although previous reports have shown that expression of PD1/PD-L1 blocking antibodies from viral vectors can provide antitumor activity in preclinical tumor models, these studies were based on the use of oncolytic viruses, such as vaccinia and measles virus.[42,43] These agents, in contrast with SFV vectors, can propagate in tumors, inducing strong antiviral responses that could limit their efficacy and prevent readministration. In addition, the presence of neutralizing antibodies against these viruses is common in the general population,[44,45] which has not been reported for SFV. Our studies comparing SFV and AAV also show that the choice of a viral vector is relevant for antitumor success, regardless of the level and duration of transgene expression.

In summary, our results show that local and short expression of immunomodulatory mAbs could be highly effective when expressed from vectors able to induce IFN-I responses, like SFV. This kind of strategy could offer a high degree of versatility, because it might allow i.t. expression of different combinations of mAbs or cytokines in a transient manner, reducing their possible toxicity.

MATERIALS AND METHODS

Cell Lines and Animals

BHK cells (ATCC-CCL10) were cultured in GMEM-BHK21 medium (Thermo Fisher, MA, USA) supplemented with 5% fetal bovine serum (FBS), 10% tryptose phosphate broth, 2 mM glutamine, 20 mM HEPES, 100 μg/mL streptomycin, and 100 U/mL penicillin (BHK complete). HEK293T (ATCC-CRL-3216) cells were cultured in DMEM medium (GIBCO) supplemented with 10% FBS, 2 mM glutamine, 100 μg/mL streptomycin, and 100 U/mL penicillin. Hamster hybridoma 10B5[3] was kindly provided by Dr. Lieping Chen (Yale University, New Haven, CT, USA) and grown in RPMI 1640 + GlutaMAX medium (GIBCO) with 10% FBS, 0.5 mM sodium pyruvate, 5 mM 2-mercaptoethanol, 1% Condimed (Roche), HT Media supplement (GIBCO), 100 μg/mL streptomycin, and 100 U/mL penicillin. MC38 cells were a kind gift from Dr. Karl E. Hellström (University of Washington, Seattle, WA, USA) and were grown in DMEM (GIBCO BRL, UK) supplemented with 10% FBS, 2 mM glutamine, and antibiotics. B16-OVA cells were kindly provided by Dr. Lieping Chen and cultured in RPMI 1640 + GlutaMAX medium supplemented with 10% FBS and 50 μM 2-mercaptoethanol. Both tumor cell lines were authenticated by Idexx Radil (Case 6592-2012) in February 2012.

Four-week-old female C57BL/6 mice were purchased from Envigo (Barcelona, Spain). Animal studies were approved by the Universidad de Navarra ethical committee (study 099-14 and 024-18) for animal experimentation under Spanish regulations.

Production of Viral Vectors

To produce AAV-aPDL1 VPs with serotype AAV8, thirty 150-cm^2 flasks containing confluent HEK293T cells were co-transfected using linear polyethylenimine 25 kDa (Polysciences, Warrington, PA, USA) with two different plasmids: pAAV-aPDL1 and pDP8.ape (Plasmid Factory, Germany), which contains adenoviral helper genes plus AAV2 rep and AAV8 cap genes. After 72 h of incubation, the supernatant was collected, treated with polyethylene glycol solution (PEG8000, 8% v/v final concentration) for 48–72 h at 4°C, and centrifuged at 3,000 rpm for 15 min. The pellet containing AAV VPs from the supernatant was resuspended in lysis buffer and kept at −80°C. Cells containing AAV VPs were collected, treated with lysis buffer (50 mM Tris-Cl, 150 mM NaCl, 2 mM $MgCl_2$, 0.1% Triton X-100), and kept at −80°C. After three cycles of freezing and thawing supernatants and cell lysates, VPs were purified by ultracentrifugation in an iodixanol gradient as described previously.[46] Finally, the purified virus was concentrated using Amicon Ultra Centrifugal Filters-Ultracel 100K (Millipore). AAV vector titers were determined by qPCR for VG copies extracted from DNase-treated VPs (High Pure Viral Nucleic Acid Kit; Roche). The primers used in the qPCR were specific for the EF1α promoter: forward-EF-866, 5′-GGTGAGTCACCCACAAAGG-3′ and reverse-EF-931, 5′-CGTGGAGTCACATGAAGCGA-3′. Vector titers obtained ranged from 1×10^{12} to 3×10^{12} VGs/mL.

SFV VPs were produced from RNA synthetized *in vitro* using plasmids pSFV-aPDL1 and pSFV-LacZ as templates. Vector RNA synthesis and transfection into BHK-21 cells by electroporation was performed as described previously.[47] For packaging SFV RNA into VPs, BHK-21 cells were co-electroporated with the recombinant RNA, together with two helper RNAs (i.e., SFV-helper-C-S219A and SFV-helper-S2 RNAs), which provided *in trans* the SFV capsid and envelope proteins, respectively.[48] SFV VPs were harvested and purified by ultracentrifugation as described previously.[49] Indirect immunofluorescence using a rabbit polyclonal antiserum specific for the nsp2 subunit of SFV replicase was used as primary antibody[50] in SFV-infected BHK-21 cells to determine the titer of each vector. Vector titers obtained were around 5–8 $\times$ 10^9 VPs/mL for SFV-aPDL1 and 2 $\times$ 10^{10} VPs/mL for SFV-LacZ.

Tumor Induction and Treatment

C57BL/6 female mice were subcutaneously injected with MC38 or B16-OVA cells (500,000 cells per animal), and vectors were administered 7–9 days after tumor inoculation. AAV-aPDL1 (10^{11} VGs), SFV-aPDL1 (3 $\times$ 10^8 VPs), and SFV-LacZ (3 $\times$ 10^8 VPs) were injected i.t. with a 28G needle in a total volume of 50 μL, using saline to dilute vectors. Negative control mice were treated with the same volume of saline. When indicated, three doses of 3 $\times$ 10^8 VPs of SFV-aPDL1 were administered i.t. every 48 h.

In experiments where mice received mAbs, the following scheme was followed: for i.t. administration of anti-PD-L1 mAb, mice received two i.t. doses of 100 ng of anti-PD-L1 mAb on days 0 and 2 after vector inoculation. For i.p. administration of anti-PD-L1, mice received three i.p. doses of 100 μg of mAb on days 0, 3, and 6. In combination studies, mice received two i.p. doses of 200 μg of anti-CD137 (clone 3H3; Bio X Cell) given on days 0 and 6 after vector inoculation. In the case of anti-LAG-3 (clone C9B7W; Bio X Cell), mice received three doses of 200 μg given on days 3, 6, and 9 after vector inoculation.

The efficacy of all treatments was evaluated every 3–4 days by measuring two perpendicular tumor diameters and considering the average diameter as an indicator of tumor size and following survival in each group.

In some experiments, tumors and blood were extracted at the indicated times after treatment. Blood samples were obtained by retro-orbital venous sinus bleeding and centrifuged at 10,000 rpm for 10 min. Tumor samples were homogenized in 250 μL of PBS-Tween 0.05% in the presence of protease inhibitor cocktail tablets (Roche, Switzerland), centrifuged at 10,000 rpm for 5 min, and supernatants were collected for ELISA analysis.

PD-L1 Binding ELISA Assay

Anti-PD-L1 mAb in supernatants from transfected (AAV) or infected (SFV) cells and in sera and tumors from treated mice was determined by a specific in-house-developed PD-L1-binding ELISA. In brief, ELISA plates were first coated with 1 μg/mL recombinant murine PD-L1 fused to human IgG1 Fc (R&D, Minneapolis, MN, USA) and incubated overnight at 4°C. We then incubated plates with serial dilutions of samples containing anti-PD-L1 mAb. Finally, plates were

incubated with a goat polyclonal secondary antibody anti-mouse IgG2a conjugated with peroxidase (Abcam, UK), and the assay was developed with tetramethylbenzidine (TMB) substrate. Then, the absorbance was measured in an ELISA reader at 450 nm. As standard curve, we used supernatant from cells transfected with pAAV-aPDL1 in which the concentration of antiPD-L1 mAb was previously quantified with a mouse IgG ELISA kit (Mabtech, Sweden).

Flow Cytometry Analysis

Tumors and TDLNs were treated with 400 U/mL collagenase D and 50 μg/mL DNase I (Roche Diagnostics, Indianapolis, IN, USA). After mechanical tissue dissociation, cells were passed through a 70-μm nylon mesh filter (BD Falcon, BD Bioscience, San Jose, CA, USA), washed, treated with ACK lysing buffer, and washed again. Blood samples were obtained as described earlier, cells were surface-stained and then fixed, and erythrocytes were cleared with FACS Lysing Solution (BD Biosciences). In all cases, a single-cell suspension was pretreated with anti-CD16/32 (clone 2.4G2; BD Pharmingen) to reduce non-specific binding to Fc receptors. After this, cells were stained with the following fluorochrome-conjugated antibodies: CD8 (clone 53-6.7), CD4 (clone RM4-5), CD62L (clone MEL-14), LAG-3 (clone C9B7W), CD137 (clone 17B51H1), OX40 (clone OX-86), PD-1 (clone RMP1-30), PD-L1 (clone 10F.9G2), TIM-3 (clone RMT3-23), ICOS (clone C398.A4), 2B4 [clone m2B4 (B6)458.1], and CD45 (clone 30F11), all of them from Biolegend (San Diego, CA, USA). To identify tumor-specific CD8 T lymphocytes, we stained cells with H-2Kb MuLV p15E Tetramer-KSPWFTTL (MBL International, Woburn, MA, USA), which comprise an epitope peptide derived from the envelope protein of an endogenous ecotropic murine leukemia virus, which is expressed in both MC38 and B16-OVA tumor cells. A FACS Canto II (BD Biosciences, Franklin Lakes, NJ, USA) was used for cell acquisition, and data analysis was carried out using FlowJo software (Tree Star, Ashland, OR, USA).

Statistical Analyses

All data are expressed as the mean ± SEM. Prism software (GraphPad Software, San Diego, CA, USA) was used for statistical analysis. Survival of tumor-bearing animals is represented by Kaplan-Meier plots and was analyzed by log-rank test. To compare experimental groups, the Kruskal-Wallis test, followed by the Dunn multiple-comparison test, was used for nonparametric data, and one-way ANOVA, followed by the Dunnett's multiple-comparison test, was used for parametric data. For time-series analysis (tumor growth curves), data were compared using the extra sum-of-squares F test in the Prism software package and fitted to a second-order polynomial equation. In Figures 1D and 1E, comparisons between saline- and vector-treated mice were done using the Mann-Whitney U test. The p values <0.05 were considered statistically significant.

Additional Materials and Methods

Determination of the anti-mouse PD-L1 mAb sequence, construction of SFV and AAV vectors, western blotting, mRNA quantitative analyses, and *in vitro* PD-L1 expression are detailed in the Supplemental Materials and Methods.

SUPPLEMENTAL INFORMATION

Supplemental Information can be found online at https://doi.org/10.1016/j.ymthe.2019.09.016.

AUTHOR CONTRIBUTIONS

Conceptualization, C.S., R.H.-A., S.H.-S., and J.P.; Methodology, M.C.B.-B., E.C., and E.M.; Investigation, M.C.B.-B., E.M., E.C., N.S.-P., M.B., J.G., U.M., J.J.L., M.G., G.K., D.E., and A.R.S.-P.; Writing – Original Draft, M.C.B.-B. and C.S.; Writing – Review & Editing, C.S., R.H.R., S.H.-S., I.M., and J.P.; Funding Acquisition, C.S., R.H.-A., S.H.-S., and J.P.; Resources, S.H.-S., J.J.L., D.E., G.K., and I.M.; Supervision, C.S., S.H.-S., and R.H.-A.

CONFLICTS OF INTEREST

I.M. reports receiving a commercial research grant from BMS, Bioncotech, Alligator, and Roche; has received speakers' bureau honoraria from MSD; and is a consultant/advisory board member for BMS, Roche, Genmab, F-Star, Bioncotech, Bayer, Alligator, and Merck Serono. The other authors declare no competing interests.

ACKNOWLEDGMENTS

We are very thankful to Dr. Lieping Chen (Yale University, New Haven, CT, USA) for providing hamster hybridoma 10B5. We also thank Eneko Elizalde and personnel at the Animal Facility of Cima Universidad de Navarra for excellent assistance, Fernando J. Corrales and Carmentxu Miqueo for help with mAb analysis, Gloria González-Aseguinolaza and her team for help in AAV production, and Esther Larrea for providing primers for IFN-I response analysis. This work was supported by the following grants: Instituto Salud Carlos III financed with Feder Funds PI17/01859 (to C.S.) and PI15/02027 (to S.H.S.), Gobierno de Navarra, Departamento de Salud 64/2019 (co-financed at 50% by the European Regional Development Fund through the FEDER Operational Program 2014-2020 of Navarra: "European Union. European Regional Development Fund. A way to make Europe" (to C.S.), "Fundacion Ramon Areces" (to S.H.-S.), and Spanish Ministry of Economy and Competitiveness SAF2015-65157-R (to R.H.-A.). M.C.B.-B. received a Fundación Echébano fellowship.

REFERENCES

1. Yang, Y. (2015). Cancer immunotherapy: harnessing the immune system to battle cancer. J. Clin. Invest. *125*, 3335–3337.
2. Melero, I., Grimaldi, A.M., Perez-Gracia, J.L., and Ascierto, P.A. (2013). Clinical development of immunostimulatory monoclonal antibodies and opportunities for combination. Clin. Cancer Res. *19*, 997–1008.
3. Dong, H., Strome, S.E., Salomao, D.R., Tamura, H., Hirano, F., Flies, D.B., Roche, P.C., Lu, J., Zhu, G., Tamada, K., et al. (2002). Tumor-associated B7-H1 promotes T-cell apoptosis: a potential mechanism of immune evasion. Nat. Med. *8*, 793–800.
4. Topalian, S.L., Drake, C.G., and Pardoll, D.M. (2015). Immune checkpoint blockade: a common denominator approach to cancer therapy. Cancer Cell *27*, 450–461.
5. Fife, B.T., Pauken, K.E., Eagar, T.N., Obu, T., Wu, J., Tang, Q., Azuma, M., Krummel, M.F., and Bluestone, J.A. (2009). Interactions between PD-1 and PD-L1 promote tolerance by blocking the TCR-induced stop signal. Nat. Immunol. *10*, 1185–1192.
6. Prasad, V., and Kaestner, V. (2017). Nivolumab and pembrolizumab: Monoclonal antibodies against programmed cell death-1 (PD-1) that are interchangeable. Semin. Oncol. *44*, 132–135.

7. Abdel-Wahab, N., Shah, M., and Suarez-Almazor, M.E. (2016). Adverse Events Associated with Immune Checkpoint Blockade in Patients with Cancer: A Systematic Review of Case Reports. PLoS ONE *11*, e0160221.

8. Wang, D.Y., Salem, J.E., Cohen, J.V., Chandra, S., Menzer, C., Ye, F., Zhao, S., Das, S., Beckermann, K.E., Ha, L., et al. (2018). Fatal Toxic Effects Associated With Immune Checkpoint Inhibitors: A Systematic Review and Meta-analysis. JAMA Oncol. *4*, 1721–1728.

9. Aznar, M.A., Tinari, N., Rullán, A.J., Sánchez-Paulete, A.R., Rodriguez-Ruiz, M.E., and Melero, I. (2017). Intratumoral delivery of immunotherapy—act locally, think globally. J. Immunol. *198*, 31–39.

10. Marabelle, A., Tselikas, L., de Baere, T., and Houot, R. (2017). Intratumoral immunotherapy: using the tumor as the remedy. Ann. Oncol. *28* (*Suppl 12*), xii33–xii43.

11. Melief, C.J. (2012). Selective activation of oxygen-deprived tumor-infiltrating lymphocytes through local intratumoral delivery of CD137 monoclonal antibodies. Cancer Discov. *2*, 586–587.

12. Ray, A., Williams, M.A., Meek, S.M., Bowen, R.C., Grossmann, K.F., Andtbacka, R.H., Bowles, T.L., Hyngstrom, J.R., Leachman, S.A., Grossman, D., et al. (2016). A phase I study of intratumoral ipilimumab and interleukin-2 in patients with advanced melanoma. Oncotarget *7*, 64390–64399.

13. Sznol, M., Ferrucci, P.F., Hogg, D., Atkins, M.B., Wolter, P., Guidoboni, M., Lebbé, C., Kirkwood, J.M., Schachter, J., Daniels, G.A., et al. (2017). Pooled Analysis Safety Profile of Nivolumab and Ipilimumab Combination Therapy in Patients With Advanced Melanoma. J. Clin. Oncol. *35*, 3815–3822.

14. Ribas, A., Dummer, R., Puzanov, I., VanderWalde, A., Andtbacka, R.H.I., Michielin, O., Olszanski, A.J., Malvehy, J., Cebon, J., Fernandez, E., et al. (2017). Oncolytic virotherapy promotes intratumoral T cell infiltration and improves Anti-PD-1 Immunotherapy. Cell *170*, 1109–1119.e10.

15. Rajani, K., Parrish, C., Kottke, T., Thompson, J., Zaidi, S., Ilett, L., Shim, K.G., Diaz, R.M., Pandha, H., Harrington, K., et al. (2016). Combination therapy with reovirus and Anti-PD-1 blockade controls tumor growth through innate and adaptive immune responses. Mol. Ther. *24*, 166–174.

16. Lichty, B.D., Breitbach, C.J., Stojdl, D.F., and Bell, J.C. (2014). Going viral with cancer immunotherapy. Nat. Rev. Cancer *14*, 559–567.

17. Bald, T., Landsberg, J., Lopez-Ramos, D., Renn, M., Glodde, N., Jansen, P., Gaffal, E., Steitz, J., Tolba, R., Kalinke, U., et al. (2014). Immune cell-poor melanomas benefit from PD-1 blockade after targeted type I IFN activation. Cancer Discov. *4*, 674–687.

18. Liljeström, P., and Garoff, H. (1991). A new generation of animal cell expression vectors based on the Semliki Forest virus replicon. Biotechnology (N. Y.) *9*, 1356–1361.

19. Quetglas, J.I., Ruiz-Guillen, M., Aranda, A., Casales, E., Bezunartea, J., and Smerdou, C. (2010). Alphavirus vectors for cancer therapy. Virus Res. *153*, 179–196.

20. Nathwani, A.C., Reiss, U.M., Tuddenham, E.G.D., Rosales, C., Chowdary, P., McIntosh, J., Della Peruta, M., Lheriteau, E., Patel, N., Raj, D., et al. (2014). Long-term safety and efficacy of factor IX gene therapy in hemophilia B. N. Engl. J. Med. *371*, 1994–2004.

21. Russell, S., Bennett, J., Wellman, J.A., Chung, D.C., Yu, Z.F., Tillman, A., Wittes, J., Pappas, J., Elci, O., McCague, S., et al. (2017). Efficacy and safety of voretigene neparvovec (AAV2-hRPE65v2) in patients with RPE65-mediated inherited retinal dystrophy: a randomised, controlled, open-label, phase 3 trial. Lancet *390*, 849–860.

22. Trapani, I., and Auricchio, A. (2018). Seeing the Light after 25 Years of Retinal Gene Therapy. Trends Mol. Med. *24*, 669–681.

23. Lin, H., Wei, S., Hurt, E.M., Green, M.D., Zhao, L., Vatan, L., Szeliga, W., Herbst, R., Harms, P.W., Fecher, L.A., et al. (2018). Host expression of PD-L1 determines efficacy of PD-L1 pathway blockade-mediated tumor regression. J. Clin. Invest. *128*, 805–815.

24. Melero, I., Quetglas, J.I., Reboredo, M., Dubrot, J., Rodriguez-Madoz, J.R., Mancheño, U., Casales, E., Riezu-Boj, J.I., Ruiz-Guillen, M., Ochoa, M.C., et al. (2015). Strict requirement for vector-induced type I interferon in efficacious antitumor responses to virally encoded IL12. Cancer Res. *75*, 497–507.

25. Woo, S.R., Turnis, M.E., Goldberg, M.V., Bankoti, J., Selby, M., Nirschl, C.J., Bettini, M.L., Gravano, D.M., Vogel, P., Liu, C.L., et al. (2012). Immune inhibitory molecules LAG-3 and PD-1 synergistically regulate T-cell function to promote tumoral immune escape. Cancer Res. *72*, 917–927.

26. Hirano, F., Kaneko, K., Tamura, H., Dong, H., Wang, S., Ichikawa, M., Rietz, C., Flies, D.B., Lau, J.S., Zhu, G., et al. (2005). Blockade of B7-H1 and PD-1 by monoclonal antibodies potentiates cancer therapeutic immunity. Cancer Res. *65*, 1089–1096.

27. Hastie, E., and Samulski, R.J. (2015). Adeno-associated virus at 50: a golden anniversary of discovery, research, and gene therapy success—a personal perspective. Hum. Gene Ther. *26*, 257–265.

28. Vanrell, L., Di Scala, M., Blanco, L., Otano, I., Gil-Farina, I., Baldim, V., Paneda, A., Berraondo, P., Beattie, S.G., Chtarto, A., et al. (2011). Development of a liver-specific Tet-on inducible system for AAV vectors and its application in the treatment of liver cancer. Mol. Ther. *19*, 1245–1253.

29. Zhu, J., Liu, J.Q., Shi, M., Cheng, X., Ding, M., Zhang, J.C., Davis, J.P., Varikuti, S., Satoskar, A.R., Lu, L., et al. (2018). IL-27 gene therapy induces depletion of Tregs and enhances the efficacy of cancer immunotherapy. JCI Insight *3*, 98745.

30. Quetglas, J.I., Rodriguez-Madoz, J.R., Bezunartea, J., Ruiz-Guillen, M., Casales, E., Medina-Echeverz, J., Prieto, J., Berraondo, P., Hervas-Stubbs, S., and Smerdou, C. (2013). Eradication of liver-implanted tumors by Semliki Forest virus expressing IL-12 requires efficient long-term immune responses. J. Immunol. *190*, 2994–3004.

31. Quetglas, J.I., Fioravanti, J., Ardaiz, N., Medina-Echeverz, J., Baraibar, I., Prieto, J., Smerdou, C., and Berraondo, P. (2012). A Semliki forest virus vector engineered to express IFNα induces efficient elimination of established tumors. Gene Ther. *19*, 271–278.

32. Sánchez-Paulete, A.R., Teijeira, Á., Quetglas, J.I., Rodríguez-Ruiz, M.E., Sánchez-Arráez, Á., Labiano, S., Etxeberria, I., Azpilikueta, A., Bolaños, E., Ballesteros-Briones, M.C., et al. (2018). Intratumoral Immunotherapy with XCL1 and sFlt3L Encoded in Recombinant Semliki Forest Virus-Derived Vectors Fosters Dendritic Cell-Mediated T-cell Cross-Priming. Cancer Res. *78*, 6643–6654.

33. Rodriguez-Madoz, J.R., Liu, K.H., Quetglas, J.I., Ruiz-Guillen, M., Otano, I., Crettaz, J., Butler, S.D., Bellezza, C.A., Dykes, N.L., Tennant, B.C., et al. (2009). Semliki forest virus expressing interleukin-12 induces antiviral and antitumoral responses in woodchucks with chronic viral hepatitis and hepatocellular carcinoma. J. Virol. *83*, 12266–12278.

34. Rodriguez-Madoz, J.R., Zabala, M., Alfaro, M., Prieto, J., Kramer, M.G., and Smerdou, C. (2014). Short-term intratumoral interleukin-12 expressed from an alphaviral vector is sufficient to induce an efficient antitumoral response against spontaneous hepatocellular carcinomas. Hum. Gene Ther. *25*, 132–143.

35. Zamarin, D., Holmgaard, R.B., Subudhi, S.K., Park, J.S., Mansour, M., Palese, P., Merghoub, T., Wolchok, J.D., and Allison, J.P. (2014). Localized oncolytic virotherapy overcomes systemic tumor resistance to immune checkpoint blockade immunotherapy. Sci. Transl. Med. *6*, 226ra32.

36. Amos, S.M., Pegram, H.J., Westwood, J.A., John, L.B., Devaud, C., Clarke, C.J., Restifo, N.P., Smyth, M.J., Darcy, P.K., and Kershaw, M.H. (2011). Adoptive immunotherapy combined with intratumoral TLR agonist delivery eradicates established melanoma in mice. Cancer Immunol. Immunother. *60*, 671–683.

37. Rodriguez-Madoz, J.R., Prieto, J., and Smerdou, C. (2005). Semliki forest virus vectors engineered to express higher IL-12 levels induce efficient elimination of murine colon adenocarcinomas. Mol. Ther. *12*, 153–163.

38. Quetglas, J.I., Dubrot, J., Bezunartea, J., Sanmamed, M.F., Hervas-Stubbs, S., Smerdou, C., and Melero, I. (2012). Immunotherapeutic synergy between anti-CD137 mAb and intratumoral administration of a cytopathic Semliki Forest virus encoding IL-12. Mol. Ther. *20*, 1664–1675.

39. Quetglas, J.I., Labiano, S., Aznar, M.A., Bolaños, E., Azpilikueta, A., Rodriguez, I., Casales, E., Sánchez-Paulete, A.R., Segura, V., Smerdou, C., and Melero, I. (2015). Virotherapy with a Semliki Forest Virus-Based Vector Encoding IL12 Synergizes with PD-1/PD-L1 Blockade. Cancer Immunol. Res. *3*, 449–454.

40. Pérez-Ruiz, E., Etxeberria, I., Rodriguez-Ruiz, M.E., and Melero, I. (2017). Anti-CD137 and PD-1/PD-L1 Antibodies En Route toward Clinical Synergy. Clin. Cancer Res. *23*, 5326–5328.

41. Vinay, D.S., and Kwon, B.S. (2016). Therapeutic potential of anti-CD137 (4-1BB) monoclonal antibodies. Expert Opin. Ther. Targets *20*, 361–373.

42. Engeland, C.E., Grossardt, C., Veinalde, R., Bossow, S., Lutz, D., Kaufmann, J.K., Shevchenko, I., Umansky, V., Nettelbeck, D.M., Weichert, W., et al. (2014). CTLA-4 and PD-L1 checkpoint blockade enhances oncolytic measles virus therapy. Mol. Ther. *22*, 1949–1959.

43. Kleinpeter, P., Fend, L., Thioudellet, C., Geist, M., Sfrontato, N., Koerper, V., Fahrner, C., Schmitt, D., Gantzer, M., Remy-Ziller, C., et al. (2016). Vectorization in an oncolytic vaccinia virus of an antibody, a Fab and a scFv against programmed cell death -1 (PD-1) allows their intratumoral delivery and an improved tumor-growth inhibition. OncoImmunology *5*, e1220467.

44. McQuillan, G.M., Kruszon-Moran, D., Hyde, T.B., Forghani, B., Bellini, W., and Dayan, G.H. (2007). Seroprevalence of measles antibody in the US population, 1999-2004. J. Infect. Dis. *196*, 1459–1464.

45. Pütz, M.M., Alberini, I., Midgley, C.M., Manini, I., Montomoli, E., and Smith, G.L. (2005). Prevalence of antibodies to Vaccinia virus after smallpox vaccination in Italy. J. Gen. Virol. *86*, 2955–2960.

46. Murillo, O., Luqui, D.M., Gazquez, C., Martinez-Espartosa, D., Navarro-Blasco, I., Monreal, J.I., Guembe, L., Moreno-Cermeño, A., Corrales, F.J., Prieto, J., et al. (2016). Long-term metabolic correction of Wilson's disease in a murine model by gene therapy. J. Hepatol. *64*, 419–426.

47. Liljestrom, P., and Garoff, H. (2003). Expression of proteins using Semliki Forest virus vectors. In Current Protocols in Molecular Biology, F.M. Ausubel, R. Brent, R.E. Kingston, D.D. Moore, J.G. Seidman, and J.A. Smith, et al., eds. (John Wiley & Sons), pp. 16.20.1–16.20.15.

48. Smerdou, C., and Liljeström, P. (1999). Two-helper RNA system for production of recombinant Semliki forest virus particles. J. Virol. *73*, 1092–1098.

49. Fleeton, M.N., Sheahan, B.J., Gould, E.A., Atkins, G.J., and Liljeström, P. (1999). Recombinant Semliki Forest virus particles encoding the prME or NS1 proteins of louping ill virus protect mice from lethal challenge. J. Gen. Virol. *80*, 1189–1198.

50. Casales, E., Rodriguez-Madoz, J.R., Ruiz-Guillen, M., Razquin, N., Cuevas, Y., Prieto, J., and Smerdou, C. (2008). Development of a new noncytopathic Semliki Forest virus vector providing high expression levels and stability. Virology *376*, 242–251.

YMTHE, Volume *27*

Supplemental Information

Short-Term Local Expression of a PD-L1 Blocking Antibody from a Self-Replicating RNA Vector Induces Potent Antitumor Responses

Maria Cristina Ballesteros-Briones, Eva Martisova, Erkuden Casales, Noelia Silva-Pilipich, Maria Buñuales, Javier Galindo, Uxua Mancheño, Marta Gorraiz, Juan J. Lasarte, Grazyna Kochan, David Escors, Alfonso R. Sanchez-Paulete, Ignacio Melero, Jesus Prieto, Ruben Hernandez-Alcoceba, Sandra Hervas-Stubbs, and Cristian Smerdou

Supplementary Materials and methods

Determination of anti-PD-L1 mAb sequence

We first determined the sequences coding for the variable regions of the heavy (HC) and light chain (LC) genes of the anti-PD-L1 mAb produced by hybridoma 10B5, derived from an Armenian hamster immunized with murine PD-L1. [1] Due to the scarce information available for hamster immunoglobulin sequences, we first purified the mAb from the hybridoma supernatant using a protein G-Sepharose column (GE Healthcare Bio-Sciences, Pittsburgh, PA). The purified anti-PD-L1 mAb was digested with trypsin and protein identification was obtained by analysis of the digests in a coupled liquid chromatography and then analyzed by tandem mass spectrometry (LC–MS/MS). This analysis allowed the identification of specific peptides from the constant regions of HC (NH_2-EDTAMYYCAR-COOH) and LC (NH_2-PPSPEELR-COOH) whose sequences were identical to those of available Armenian hamster mAb sequences. [2-3] With this information, specific oligonucleotides were designed for the anti-PD-L1 mAb HC and LC sequences that allowed to reverse transcribe and amplify their mRNAs. Briefly, total RNA was purified from 10B5 hybridoma using the RNeasy kit (Qiagen) and the 5´end of HC and LC mRNAs were reversed transcribed using reverse sense oligonucleotides (for HC: 5´-TCTTGCACAGTAGTACATGG-3´ and for LC: 5´-CCGGAGCTCCTCAGGTGAAG-3´) and amplified by PCR using the 5' RACE System for Rapid Amplification of cDNA Ends (ThermoFisher, Waltham, MA). Since the peptide identifed for HC was in a conserved area within the variable region, the 3´end of its mRNA was also amplified by reverse transcribing total mRNA with a poly-dT oligonucleotide and performing a PCR with the specific forward primer 5´- GAGGACACAGCCATGTACTAC-3´, which sequence was based on the identified HC peptide. In each case, amplified DNA fragments from at least three independent PCR reactions were sequenced, allowing to

determine the nucleotide and amino acid sequences of the variable regions of the anti-PD-L1 LC and HC chains (see next part).

Construction of AAV and SFV vectors expressing anti PD-L1 mAb

A synthetic anti-PD-L1 codon-optimized sequence containing the mAb variable regions described in the previous part and mouse IgG2a and lambda2 constant regions, for HC and LC chains, respectively, was obtained from GenScript (Nanjing, China) cloned in pUC57 flanked by EcoR V sites (pU57-aPDL1). The HC and LC amino acid sequences encoded in this plasmid are the following:

HC: NH_2-MNWGLKLVFFVLILKGVQC**EVQLVESGGGLEQPGKSLKLSCEAS-GFTFSDYYMSWVRQAPGKGLEWVAYISSGSSNIKYVDVVKGRVTISRDNAKNLL SLQMNNLKSEDTAMYYCARGGYALDFWGQGTQVTVSS***AKTTPPSVYPLAPGSAAQ TNSMVTLGCLVKGYFPEPVTVTWNSGSLSSGVHTFPAVLQSDLYTLSSSVTVPSSTWPSETV TCNVAHPASSTKVDKKIVPRDCGCKPCICTVPEVSSVFIFPPKPKDVLTITLTPKVTCVVVDI SKDDPEVQFSWFVDDVEVHTAQTQPREEQFNSTFRSVSELPIMHQDWLNGKEFKCRVNS AAFPAPIEKTISKTKGRPKAPQVYTIPPPKEQMAKDKVSLTCMITDFFPEDITVEWQWNGQ PAENYKNTQPIMDTDGSYFVYSKLNVQKSNWEAGNTFTCSVLHEGLHNHHTEKSLSHSPG K*-COOH

LC: NH_2-AWIPLLLLFFHCTGSFSQ**PLLTQSPSASASLGNSVKITCTLSSQHSTY-GIRWYQQHPDKAPKYVMFVTSDGSHGKGDGIPDRFSGSSSGAHRYLSISNIQSED EADYYCGTGDSTGFVFGSGTQLTVL***GQPKSTPTLTVFPPSSEELKENKATLVCLISNFS PSGVTVAWKANGTPITQGVDTSNPTKEGNKFMASSFLHLTSDQWRSHNSFTCQVTHEGDT VEKSLSPAECL*-COOH

The variable regions of each antiPD-L1 mAb chain are indicated in bold with their signal peptides underlined, while the murine-derived constant regions are indicated in italics.

Plasmid pU57-aPDL1 contained the HC and LC mAb sequences fused by the sequence of 2A autoprotease from foot-and-mouth disease virus (2A), including a furin cleaving site at the carboxyl terminus of the HC, a strategy described earlier for efficient antibody expression [4] (Fig. 1A).

To generate the AAV-aPDL1 plasmid (pAAV-aPDL1), a DNA fragment containing anti-PDL1 mAb sequence was obtained by EcoR V digestion from pUC57-aPDL1 and subcloned under the control of human elongation factor 1 alpha (EF1α) promoter into AAV2 DNA backbone using a pAAV2 plasmid (Agilent Technologies, Sant Clara, CA).

To generate the SFV-aPDL1 vector the anti-PD-L1 mAb sequence was first amplified by PCR from pAAV-aPDL1 with the following primers: Forward: 5´GAGCGGGCCCAATTGGGGACTGAAACTCG3´ and Reverse: 5´GAGCGGGCCCCTA GAGACATTCTGCTGG3´. These primers contained an Apa I site (underlined) which allowed subcloning of the PCR fragment into the Apa I site into pSFVb1-2A [5] in frame with the minimal SFV capsid translation enhancer (b1), using the 2A autoprotease as a linker. Plasmid pSFV-LacZ has been described previously. [6]

Analysis of protein expression by Western Blot

BHK-21 cells were transfected with pAAV-aPDL1 or infected with SFV-aPDL1 (the infectivity of AAV *in vitro* is very inefficient, so the expression of the mAb was analyzed by transfecting the plasmid containing the vector). For transfection, BHK cells were cultured in 6-well plates and incubated with 300 µl of Optimem medium (Invitrogen) containing 2 µg of pAAV-aPDL1 and 5 µl of lipofectamine 2000 (Invitrogen). For infection, confluent BHK cells monolayers were incubated with SFV VPs at a multiplicity of infection of 10 and diluted in 300 µl of MEM medium (Gibco BRL, UK) containing 0.2% bovine serum albumin, 2 mM glutamine and 20 mM Hepes. In both cases (transfection and infection), medium was

removed after 1 h at 37º and cells were incubated for 24h at 37ºC with CHO medium without FBS (Sigma, St. Louis, MO). Supernatants were analysed by Western blot under reducing (with dithiothreitol, DTT) and non-reducing (without DTT) conditions in 12% or 8% polyacrylamide gels, respectively. Anti-PD-L1 mAb was visualized by incubating with a polyclonal goat antibody specific for mouse IgG conjugated with peroxidase (Sigma).

Analysis of mRNA in tumors by RT-qPCR

Tumors were extracted 17h after treatment, homogenized at 4ºC, and total RNA was purified using Maxwell® RSC simplyRNA Cells Kit (Promega, Madison, WI), according to the manufacturer's instructions. DNase I-treated RNA was retrotranscribed to cDNA using random primers (Promega) with M-MLV reverse transcriptase in the presence of RNase OUT (Invitrogen, Carlsbad, CA). For quantitative PCR, cDNAs were amplified using iQ SYBR ® Green Supermix in a C1000 thermal cycler according to the manufacturer's instructions (Bio-Rad, Hercules, CA). cDNAs were amplified with oligonuclotides specific for the following mouse genes: GAPDH (forward: 5´-TGCACCACCAACTGCTTA-3´; reverse: 5´-CAGAAGACTGTGGATGGCCCCTC-3´), 2'-5'-oligoadenylate synthetase 2 (forward: 5´-ACTGTCTGAAGCAGATTGCG-3´; reverse: 5´-TGGAACTGTTGGAAGCAGTC-3´), TRIM-21 (forward: 5´-GCTTCACCTATTCTGTGAGG-3´ ; reverse: 5´-ATCCATTTCCATCTTCTCGG-3´), STAT-I (forward: 5´-TCATCAGTCACCAAGAGAGG -3´ ; reverse: 5´- ATCATTCCAGAGGCACAG -3´), Mx1 (forward: 5´-ATCTGTGCAGGCACTATGAG-3´ ; reverse: 5´- CCTTCCTTCTTTACGCTTCC-3´), and for SFV replicase (forward: 5´-CTGTTCTCGACGCGTCGTC-3´ ; reverse: 5´-GAGGTGTTTCCACGACCC-3´). Relative levels for each RNA were determined with following formula: $2^{\Delta Ct}$ where ΔCt = Ct (GAPDH) – Ct (gene of interest).

Analysis of PD-L1 expression *in vitro*

MC38 and B16-OVA cells were plated in 12-well plates ($5x10^4$ cells/well) and cultured as described during 6h. Then, medium was replaced by new medium containing 100 units/ml of murine IFNγ (Miltenyi, Germany) and incubated for 48h. At that time, cells were collected using diluted trypsin (1:4) and analyzed by flow cytometry as described, using PE-conjugated anti-mouse PD-L1 antibody (Biolegend, clone 10F.9G2).

Supplementary Figure legends

Supplementary Figure S1. Evaluation of antitumor efficacy of SFV-aPDL1 in mice with two MC38 subcutaneous tumors. C57BL/6 mice were inoculated subcutaneously with $5x10^5$ and $3x10^5$ MC38 cells in the lateral and contralateral flanks, respectively. Approximately seven days later (day 0), animals received one intratumoral dose of SFV-aPDL1 ($3x10^8$ VPs) or saline in the lateral tumor (treated), while the contralateral tumor was left untreated. **A**, Evolution of tumor size. Data represent the mean tumor size (mm^2) + SEM. **B**, Survival after treatment. *, $p < 0.05$; ***, $p < 0.001$; ****, $p < 0.0001$.

Supplementary Figure S2. Evaluation of the antitumor effect of SFV-aPDL1 in C57BL/6 mice carrying subcutaneous B16-OVA tumors. $5x10^5$ B16/OVA cells were inoculated subcutaneously into the right flank of C57BL/6 mice and six days later, when tumors had an average diameter of 4-5 mm, animals received one intratumoral dose of $3x10^8$ VPs of the indicated SFV-derived vectors or an equivalent volume of saline. **A**, Evaluation of tumor size (mm^2) for each individual mouse. The fractions in the right corner of each graph indicate the number of complete regressions/total number of mice for each group. **B**, Mean tumor size evolution + SEM. Data are represented only until day 7 since saline mice had to sacrificed at

this time point due to tumor size or ulceration. **C**, Survival after treatment. ***, p <0.001; ****, p <0.0001, ns not significant.

Supplementary Figure S3. Evaluation of SFV-LacZ in combination with anti-PDL1 mAb given IP. C57BL/6 mice bearing subcutaneous tumors were inoculated with SFV-LacZ ($3x10^8$ VPs) IT, with anti-PDL1 mAb (BioXcell. Clon 10F.9G2) given IP as described in Fig. 3, or with a combination of both agents. Mice treated with saline were used as negative control. **A**, Evolution of tumor size (mm^2) along time for each individual mouse. The fractions in the right lower corner of each graph indicate the number of complete regressions/total number of mice in each group. Dashed lines indicate the times of mAb administrations. **B**, Mean tumor size evolution ± SEM. **C**, Survival after treatment. +, p=0.07, *, p <0.05; **, p <0.01; ***, p<0.001****, p<0.0001; ns, not significant.

Supplementary Figure S4. Analysis of PD-L1 expression in tumor cells. (**A**) MC38 and B16-OVA cells were cultured in presence or absence of 100 units/ml of murine IFNγ, incubated for 48h and analyzed by flow cytometry with anti-mouse PD-L1 antibody (n=3). (**B**) C57BL/6 mice bearing subcutaneous MC38 or B16-OVA tumors (n=4-6) were inoculated with the indicated vectors or saline as described in Fig. 5. Five days after treatment tumors were excised, digested and cells were stained for surface marker PD-L1 and analysed by flow cytometry. PD-L1 levels were evaluated in total CD45-negative cells (tumor cells). Histograms to the left of each graph show the expression of PD-L1 on tumor cells as observed in one representative well per condition. **, p <0.01; ****, p<0.0001; ns, not significant.

Supplementary Figure S5. Analysis of CD62L in tumor CD8 T cells. C57BL/6 mice bearing subcutaneous MC38 (**A**) or B16-OVA (**B**) tumors were inoculated with the indicated

vectors or PBS as described in Fig. 5 (MC38) and 7 (B16-OVA). Five days after treatment tumors were excised, digested and freshly purified lymphocytes were stained for surface marker CD62L and analysed by flow cytometry. CD62L levels were evaluated in total CD8 T cells (left graphs) and tumor-specific CD8 T cells ($Tetr^+$) (right graphs). Data represent mean ± SEM (n=6). Asterisks above each bar indicate the statistical comparison of each group with control saline group. Other comparisons are indicated by horizontal bars. *, $p<0.05$; **, $p<0.01$, ns, not significant.

Supplementary Figure S6. Analysis of additional co-stimulatory and co-inhibitory immunological markers in MC38 tumor T cells. Freshly purified lymphocytes were collected from tumors as described in Fig. 5 and analysed by flow cytometry with antibodies specific for the immunological co-stimulatory marker ICOS (**A**), and for immunological co-inhibitory markers TIM3 (**B**) and 2B4 (**C**). Data show levels of each marker in total CD8 cells (left graphs), MC38-specific CD8 T cells (central graphs), and total CD4 T cells (right graphs). Asterisks above bars indicate the statistical comparison of each group with control saline group. Other comparisons are indicated by horizontal bars. *, $p<0.05$; ns, not significant.

Supplementary Figure S7. Analyses of co-stimulatory and co-inhibitory immunological markers on B16-OVA tumor T cells. Tumor-infiltrating lymphocytes obtained as described in Fig. 7 were analyzed by flow cytometry with antibodies specific for the immunological co-inhibitory markers PD-1 (**A**), LAG3 (**B**), and co-stimulatory marker CD137 (**C**). Data show levels (mean ± SEM, n=6) of each marker in total CD8 T cells (left graphs), tumor-specific CD8 T cells (B16-$Tetr^+$, central graphs), and total CD4 T cells (right graphs). Asterisks above

each bar indicate the statistical comparison of each group with control saline group. Other comparisons are indicated by horizontal bars. *, $p<0.05$; ns, not significant.

Supplementary Figure S8. Analyis of CD137 and PD-1 co-expression in MC38 tumors. Tumor-infiltrating lymphocytes were obtained from non-treated MC38 tumors and analyzed by flow cytometry with antibodies specific for PD-1 and CD137. (**A**) The right graph represents the percentage of double positive PD1+ CD137+ in total or tumor specific CD8 cells (MC38 Tetr+). Dot plots show representative gating strategies for the indicated cells. (**B**) Percentage of CD137+ CD8 cells which are PD-1+ or PD-1- (inidcated in the X axis). Data show mean ± SEM, n=6. ****, $p<0.0001$.

Supplementary Figure S9. Gating strategy used to identify CD4 and CD8 T cells in the tumor microenvironment. Lymphocytes were gated from CD45+ cells based on FSC and SSC (**A**). Next, dead cells were removed from the analysis using Zombi NIR fixable dead cell stain (**B**). Doublets were removed from lymphocytes using FSC-A and FSC-H (**C**). Plot in **D** shows CD4+ and CD8+ cell gates and plot in **E** depict Tetramer+ (Tetr) cells in CD8 TILs. Plot Titers refer to the gated population exhibited.

Supplementary References

1. Dong H., Strome S.E., Salomao D.R., Tamura H., Hirano F., Flies D.B. *et al.* (2002). Tumor-associated B7-H1 promotes T-cell apoptosis: a potential mechanism of immune evasion. Nat. Med. 8, 793-800.

2. Verdino P., Witherden D.A., Podshivalova K., Rieder S.E., Havran W.L., Wilson I.A. (2011). cDNA sequence and Fab crystal structure of HL4E10, a hamster IgG lambda light chain antibody stimulatory for gammadelta T cells. PLoS One 6, e19828.

3. Haggart R., Perera J., Huang H.C. (2013). Cloning of a hamster anti-mouse CD79B antibody sequences and identification of a new hamster immunoglobulin lambda constant IGLC gene region. Immunogenetics 65, 473-478.

4. Fang J., Qian J.J., Yi S., Harding T.C., Tu G.H., VanRoey M. *et al.* (2005). Stable antibody expression at therapeutic levels using the 2A peptide. Nat. Biotechnol. 23, 584-590.

5. Rodriguez-Madoz J.R., Prieto J., Smerdou C. (2005). Semliki forest virus vectors engineered to express higher IL-12 levels induce efficient elimination of murine colon adenocarcinomas. Mol. Ther. 12, 153-163.

6. Quetglas J.I., Fioravanti J., Ardaiz N., Medina-Echeverz J., Baraibar I., Prieto J. *et al.* (2012). A Semliki forest virus vector engineered to express IFNalpha induces efficient elimination of established tumors. Gene. Ther. 19, 271-278.

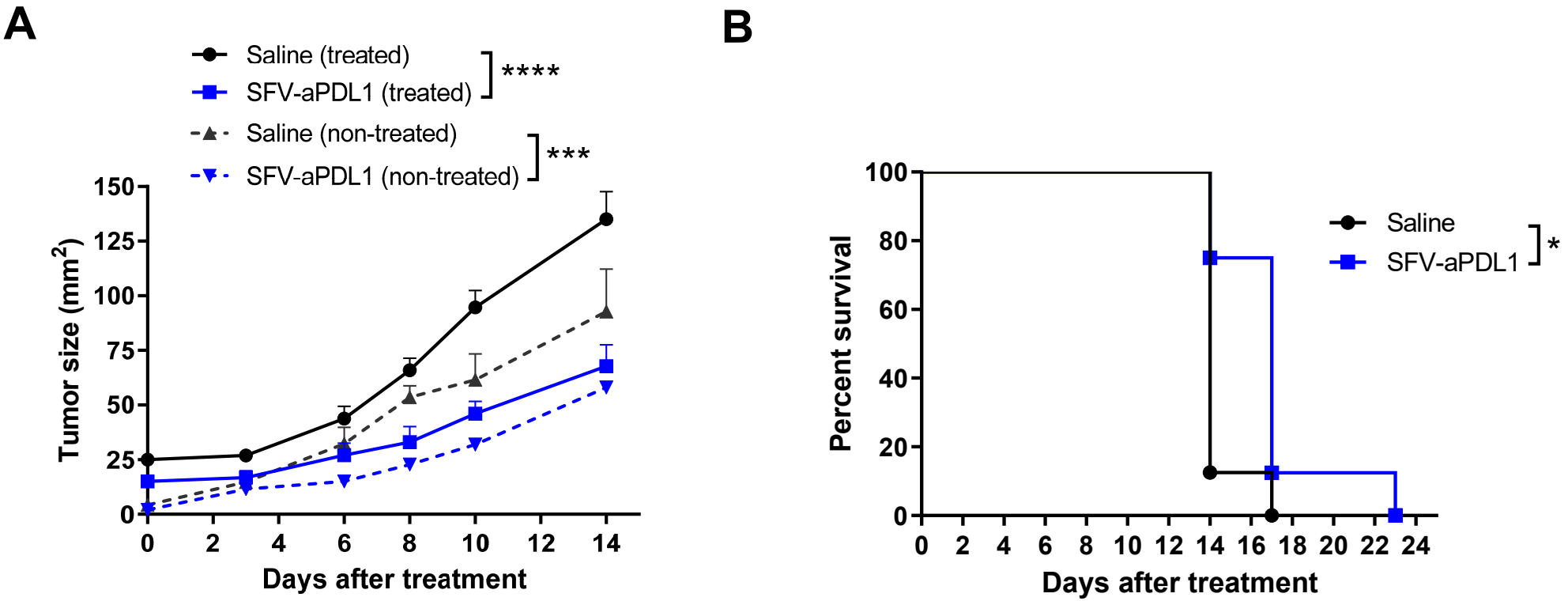

Supplementary Figure S1

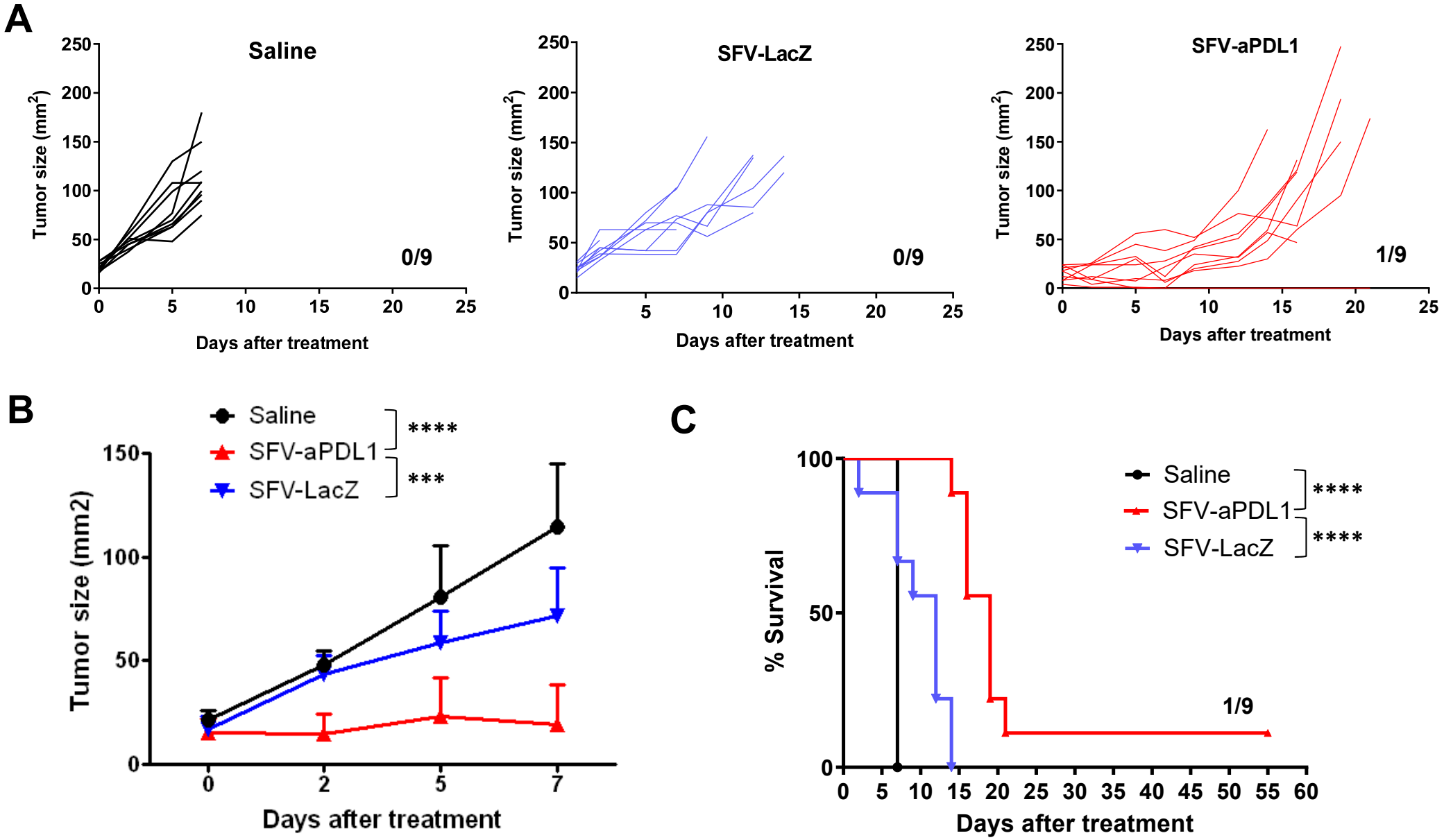

Supplementary Figure S2

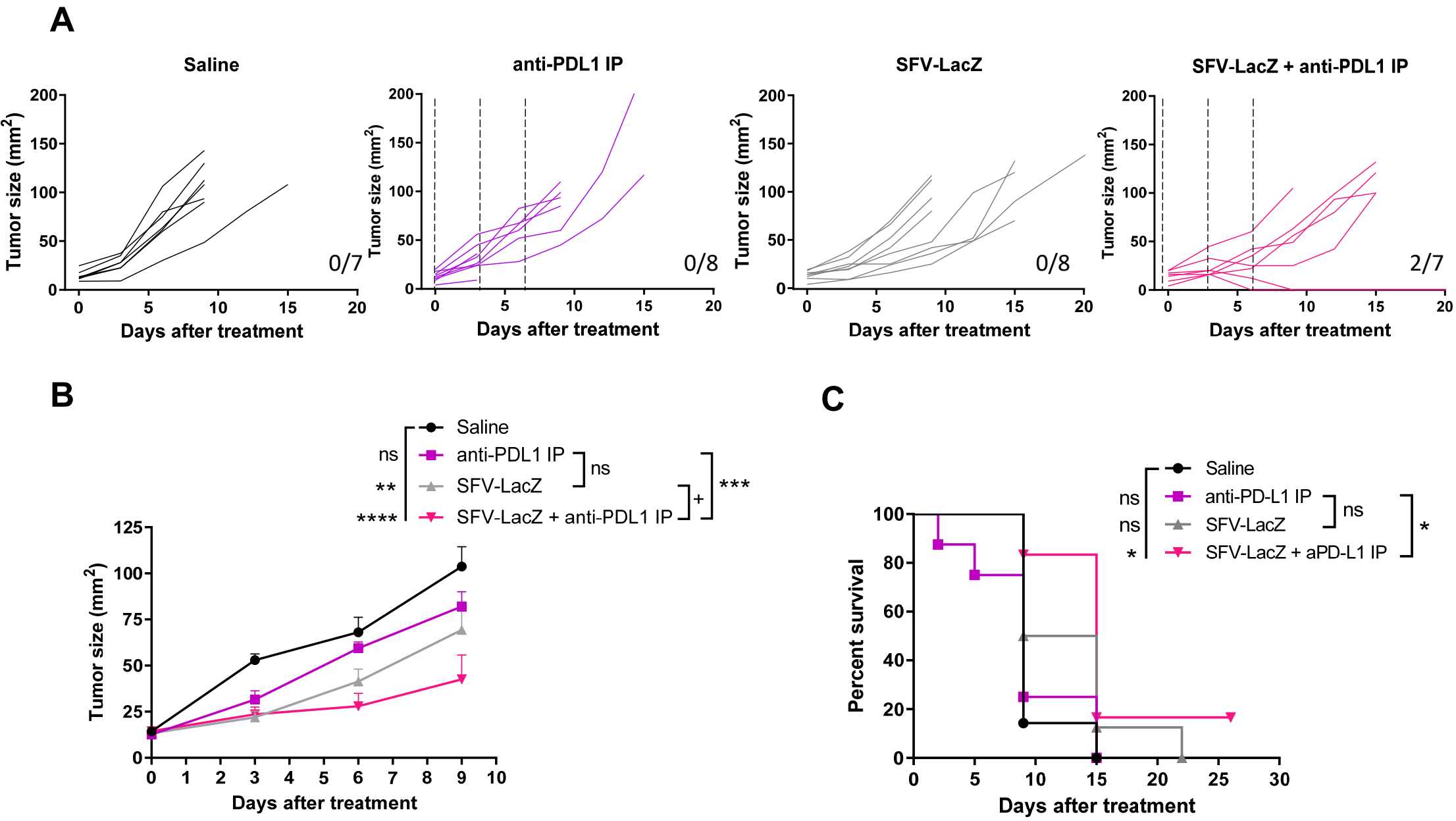

Supplementary Figure S3

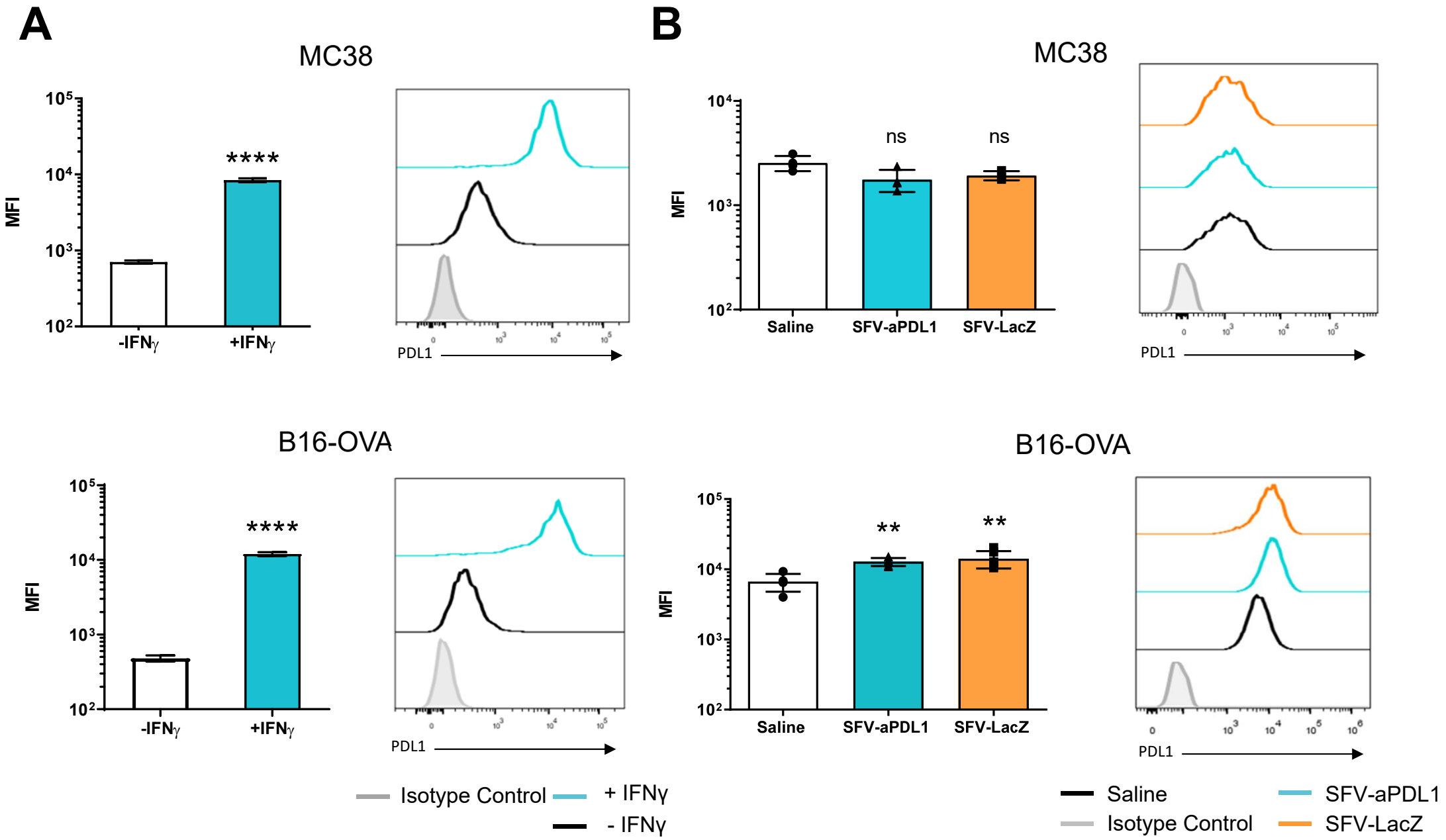

Supplementary Figure S4

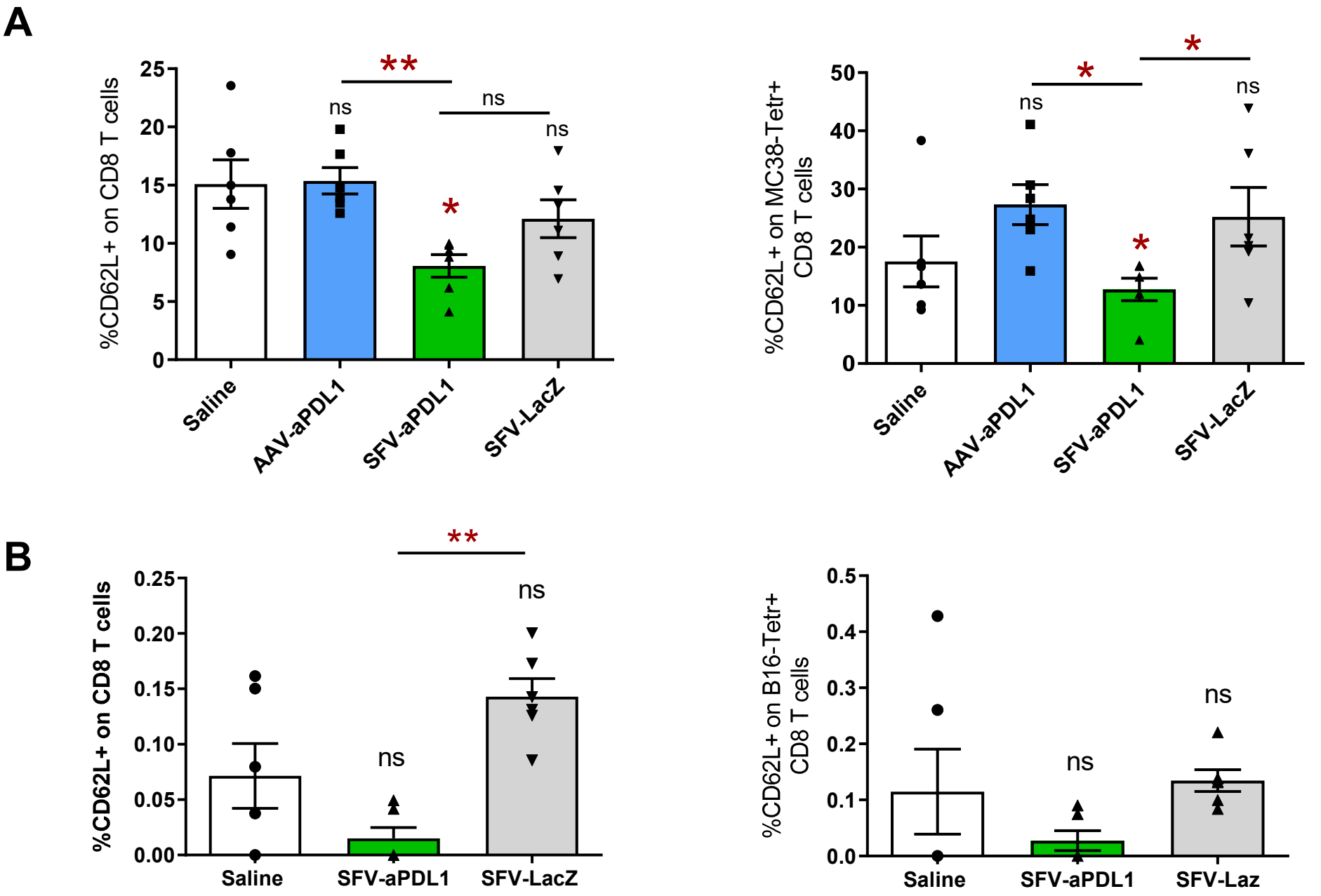

Supplementary Figure S5

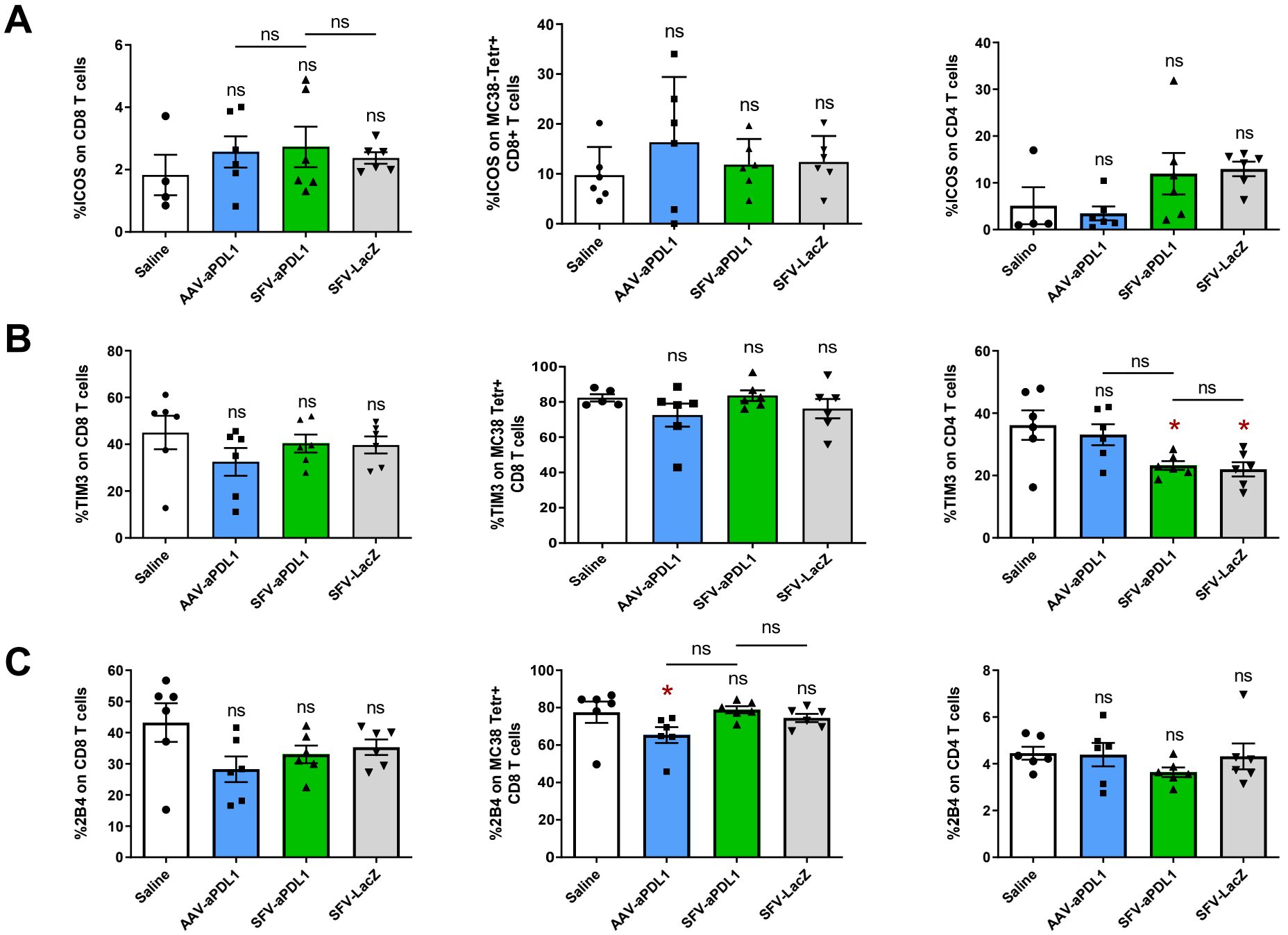

Supplementary Figure S6

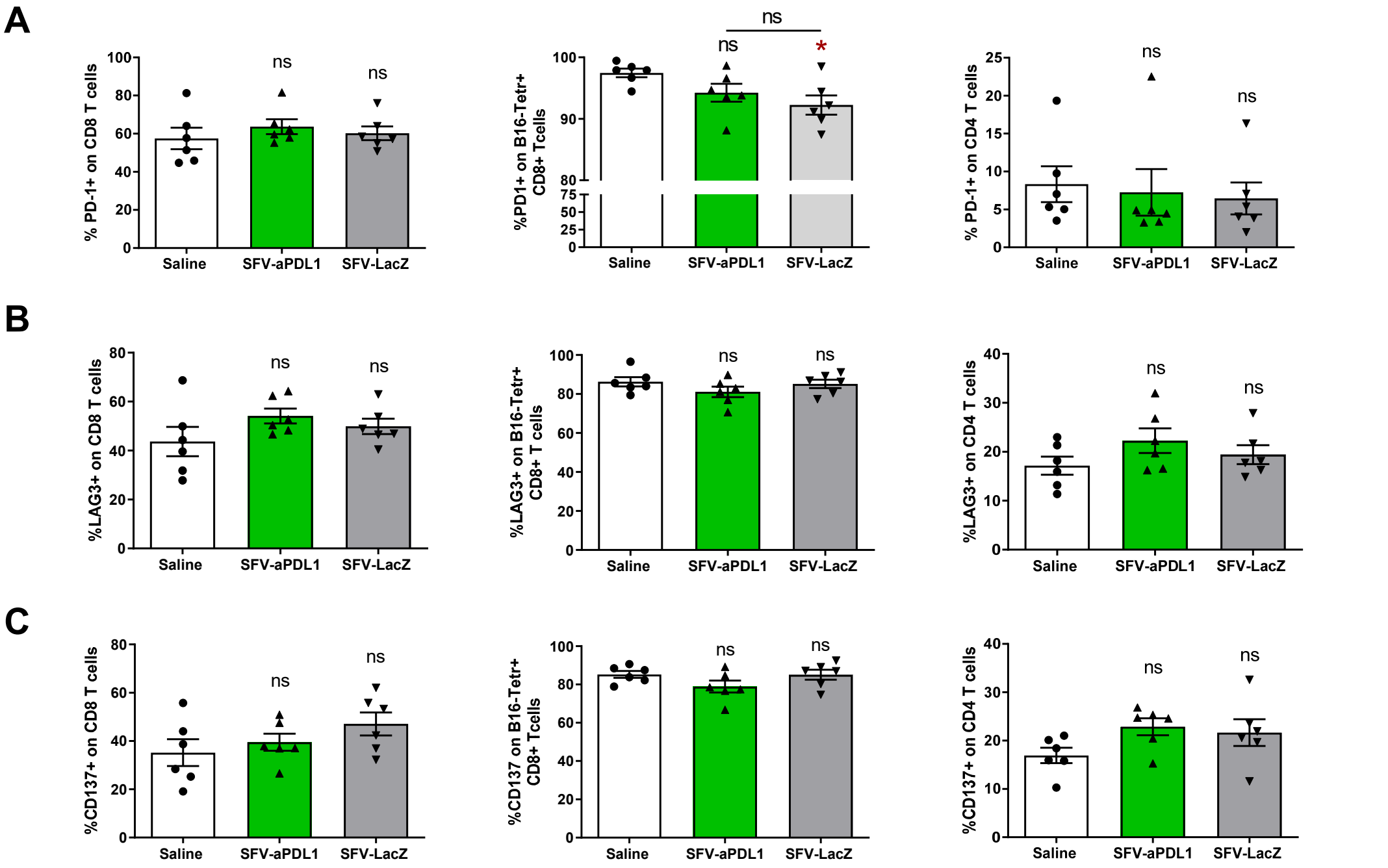

Supplementary Figure S7

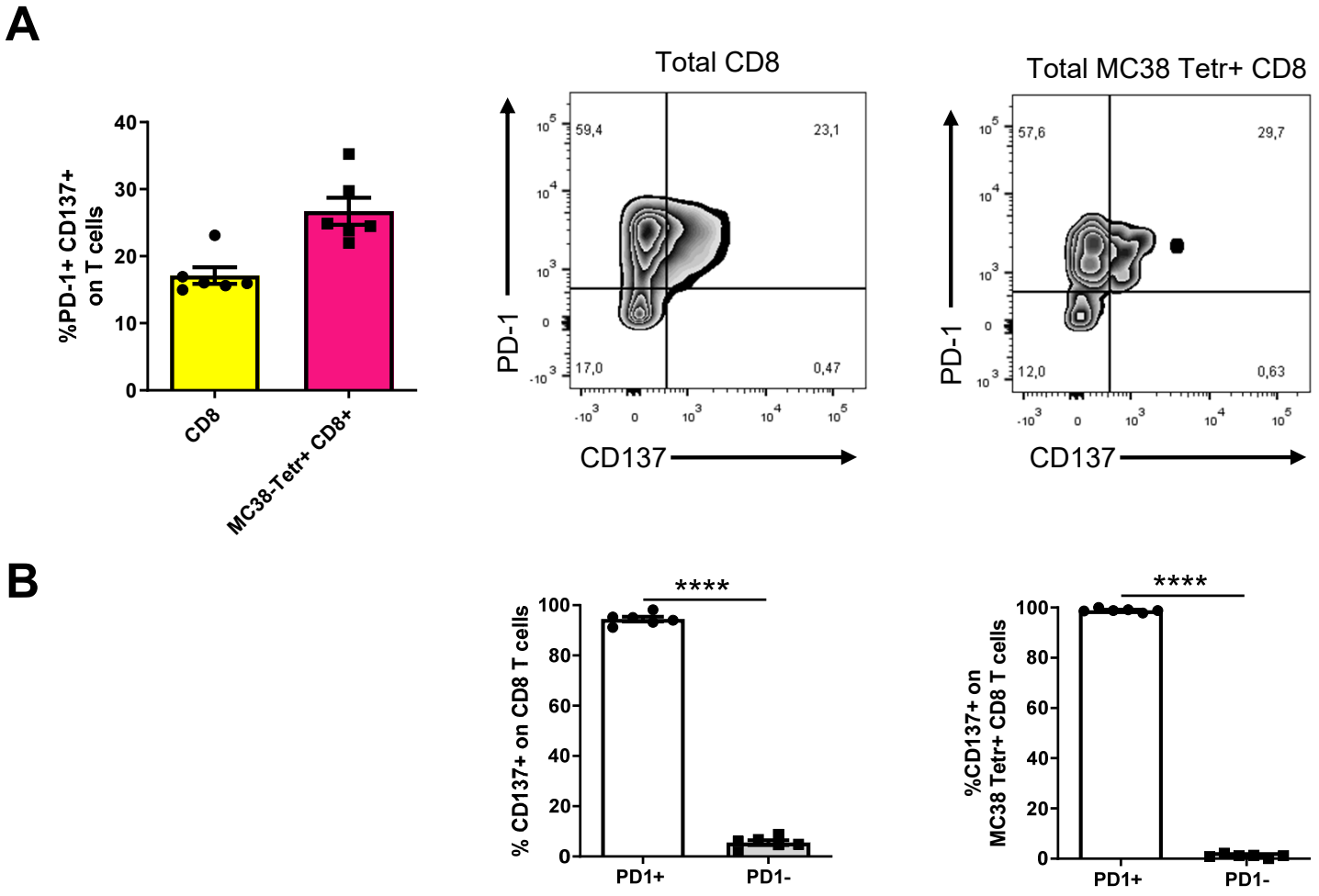

Supplementary Figure S8

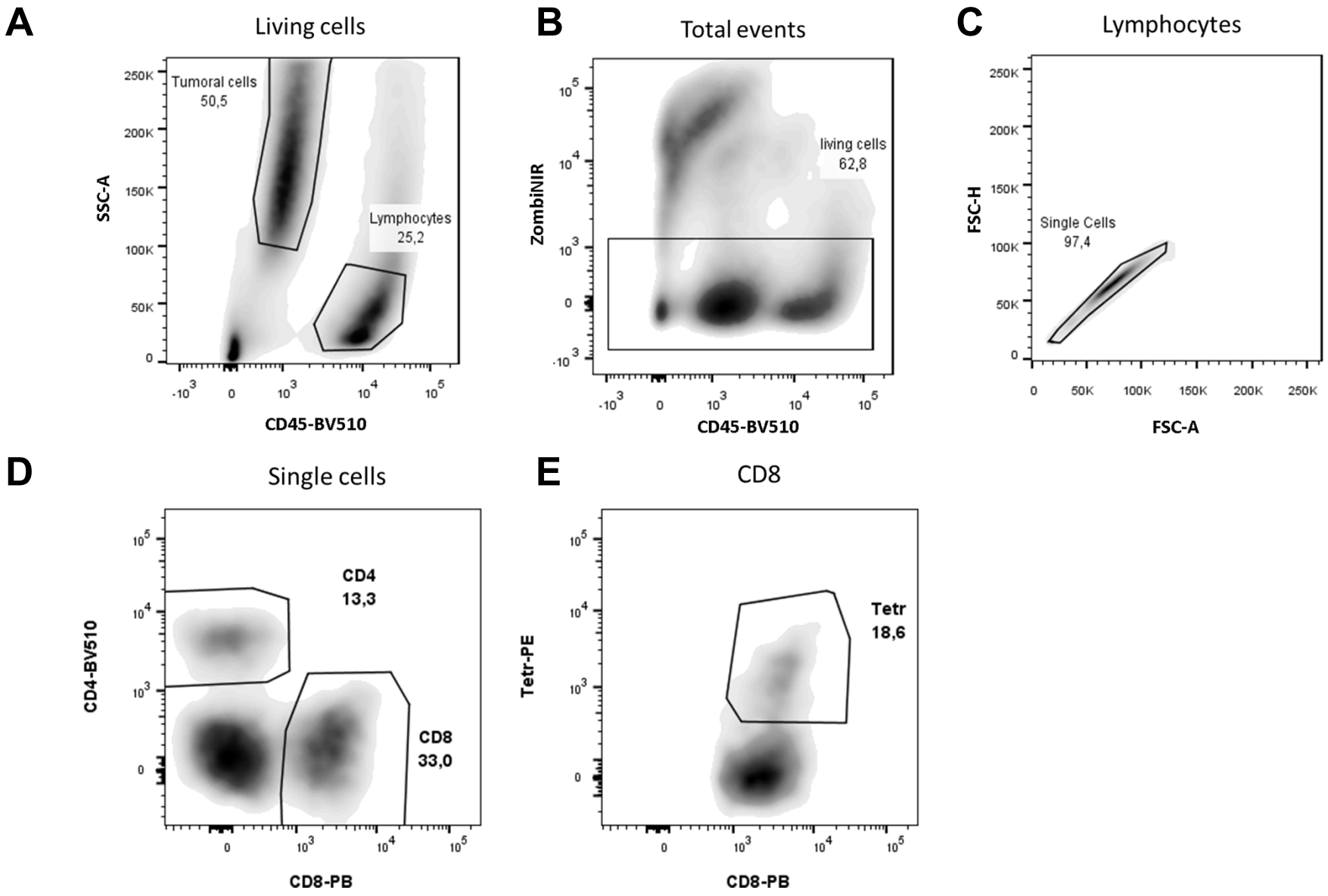

Supplementary Figure S9